Automation and Optimization of Computer-Assisted Surgery Planning of Corrective Osteotomies for Forearm Malunions

MSc Thesis Technical Medicine

F.M.A. Koopman

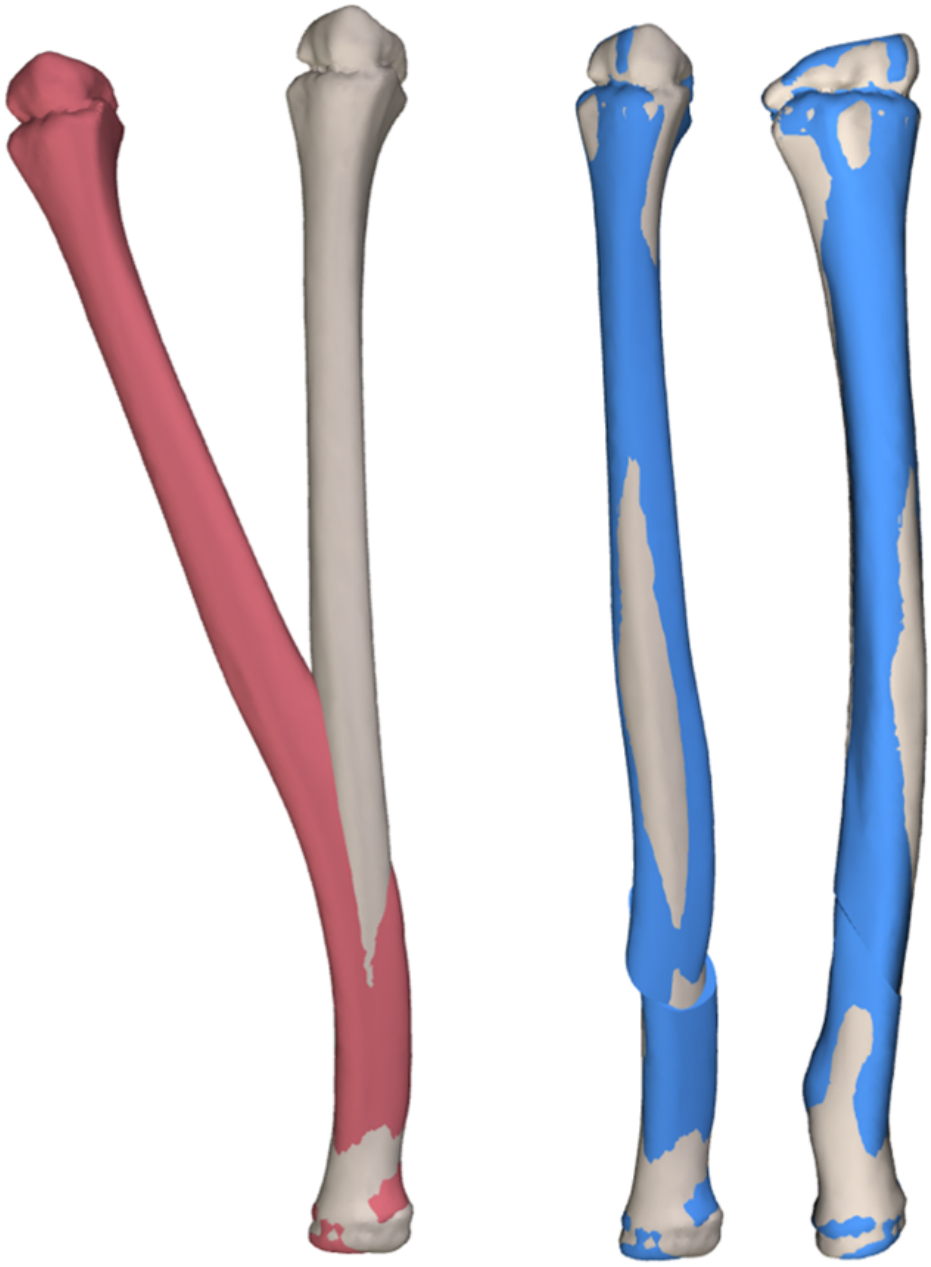

TU Delft

Erasmus MC
University Medical Center Rotterdam

Automation and Optimization of Computer-Assisted Surgery Planning of Corrective Osteotomies for Forearm Malunions

by

F.M.A. Koopman

Frédérique 4470885

Technical Supervisor:	dr. ir. B. L. Kaptein
Medical Supervisor:	dr. J. W. Colaris
Daily Supervisor:	drs. E. M. van Es
Project Duration:	14.02.2023 - 06.06.2023
Faculty:	Faculty of Mechanical, Maritime and Materials Engineering, Delft

TU Delft

Summary

Corrective osteotomies are the indicated treatment for complex forearm malunions. The use of 3D computer-assisted preoperative planning offers significant advantages, such as improved comprehension of the multiplanar deformity and high accuracy. However, the clinical application of computer-assisted preoperative planning methods is limited due to the considerable time, effort, and expertise required. This emphasizes the necessity for a tool that can generate clinically feasible osteotomy plans, complying with patient-specific anatomical reconstruction goals. To address this challenge, this research developed an automatic planning tool for corrective osteotomies of radius malunions, requiring minimal user interaction. By automatically registering the pathological and contralateral bone models, the tool provides insight into the degree and nature of the deformity. An Evolutionary Algorithm is implemented to optimize patient-specific osteotomy plans by minimizing bone protrusion near the osteotomy plane. The automatic planning tool yields patient-specific osteotomy plans including the osteotomy plane location and orientation, as well as the required reduction of the distal part after the osteotomy cut. These plans ensure accurate alignment of both the proximal and distal radial joint surfaces. The developed tool was validated on 15 patient cases. The osteotomy plans generated by the automatic tool were compared to those planned manually in the past. Objective validation, based on residual alignment errors of the entire radius bone, often favored the manual planning approach. However, the automatic tool consistently provided osteotomy plans with more accurate alignment of the distal joint surface. Additionally, a blinded qualitative validation was conducted with a highly experienced orthopedic surgeon, who rated all osteotomy plans on a scale of 1 to 10. The results indicated that the automatic tool is not yet capable of generating osteotomy plans with feasibility scores equivalent to manual planning. However, the feasibility scores differed by only one point on most patient cases. The main areas that require improvement to consistently produce clinically feasible osteotomy plans include the incorporation of osteosynthesis plate fixation, consideration of the relationship with the ulna, and the option for double-cut osteotomies. In conclusion, the developed tool is capable of generating clinically feasible osteotomy plans, serving as a valuable starting point for patient-specific plans that can be further refined manually.

Acknowledgments

This master's thesis is the result of 9 months of research and with that it concludes my Master's degree in Technical Medicine at the TU Delft, the Erasmus University, and the Leiden University. This project allowed me to delve deeply into automation and optimization of 3D computer-assisted surgery planning, a topic I have been interested in since following the like-named course. It have been a challenging yet rewarding 9 months.

I would like to express my gratitude to my three supervisors, Bart Kaptein, Joost Colaris, and Eline van Es. I enjoyed our regular meetings, discussing the project and your perspectives on it from different point-of-views. Every meeting gave me new and insightful ideas to help me move forward. Your guidance throughout the project was a valuable combination of knowledge from different disciplines, something highly relevant for a Technical Medicine project. It helped me to constantly keep improving my work. You guided me through the project with thoughtful suggestions and realistic feedback while also providing me with the time and space to learn from it myself. Bart, your extensive knowledge and expertise always helped me to gain a thorough understanding of the different aspects of this project. I appreciate your patience and how you always made time for discussions about transformation matrices and optimization algorithms, from which I learned a lot. Joost, your enthusiasm for this topic as a clinician has worked highly motivating for me and your confidence in the added value of projects like this makes me excited for the future. I learned a lot during the outpatient clinics by seeing the clinical side of this project. Eline, I am grateful for the approachable contact and for you teaching me the practical side 3D planning. Your experience was instrumental in providing me with a perspective throughout the project to prioritize the clinical rationale.

I would also like to thank my family and friends for their support and understanding during this thesis. I really appreciate the interest you all had in my project. A special thanks to Vera, for our numerous conversations and coffee breaks that kept us motivated. I am glad we got to support each other from the first day to the the 6th of june. Also thank you Emiel, for proofreading my thesis and for encouraging me through all phases.

I can honestly say I enjoyed doing this thesis and I hope that it will eventually contribute to a wider implementation of computer-assisted reconstructive surgery. Even more, I hope that it will not only showcase its benefits within the specific context but also underscore the added value that technical applications bring to the field of medicine.

Frédérique Koopman

23 May 2023

Contents

List of Figures

List of Tables

1 Introduction

The forearm consists of two bones: the radius and the ulna. The two bones are dependent and dynamic, as the radius rotates around the ulna during pro- and supination [3]. Several structures between the radius and the ulna provide the articulation between the two bones, making it a complex functional unit [4]. When the forearm is fractured and does not heal properly, a malunion can occur. This results in a deformity of the bone or an abnormal bone position. Post-traumatic malunions of the forearm can lead to impaired function due to pain, a limited range of motion, instability, and loss of strength [5–7]. Moreover, aesthetic problems can arise from malunions. Malunions can also increase the risk for osteoarthritis, especially when intra-articular structures are involved [4]. For malunions, a corrective osteotomy is the indicated treatment to restore the bony anatomy [8]. Often, malunions of the forearm are complex 3D deformations, requiring a challenging multidimensional reconstruction. The reconstruction of the malunited forearm requires a thorough understanding of the normal as well as pathological anatomy, combined with a comprehensive clinical assessment and acquisition of appropriate imaging [9]. However, the multiplanar complexity of the deformation is not always recognized on conventional 2D radiographs. Even on CT imaging, it can be hard to get an accurate overview of the 3D anatomy of the malunion. Another great challenge is determining the osteotomy plan: the location of the osteotomy cut and the orientation of the cutting plane relative to the bone. These factors make the preoperative planning of corrective osteotomies extremely challenging [10]. Even more demanding is being able to physically reproduce the osteotomy as planned [11]. Nevertheless, a positive correlation between higher accuracy of anatomical correction and better functional outcomes has been found [12, 13], emphasizing the importance of a comprehensive understanding of the patient's malunion anatomy.

3D computer-assisted planning has emerged as the state-of-the-art treatment in complex surgeries for bone deformities [14]. Multiple studies have demonstrated that the use of 3D computer-assisted planning has improved the surgeon's understanding of complex malunions [15]. In computer-assisted planning, CT data is segmented and 3D surface (STL) models are reconstructed using the Marching Cubes algorithm in a virtual environment [16]. These 3D models are used to give the surgeon a more complete, detailed preoperative insight into the complex anatomy of the malunion. In addition, the 3D model of the contralateral bone can be mirrored and used as a reference model [11]. Consequently, computer-assisted planning allows for the planning of the bone correction. The position of the osteosynthesis plate can also be planned. Computer-assisted planning also enables the design of patient-specific surgery guides, facilitating the transfer of the virtual surgery planning to the real corrective surgery. Altogether, this brings the ability to evaluate the anatomical reconstruction outcome before the physical surgery.

3D computer-assisted planning has been proven to reduce the operation time, blood loss volume, and radiation exposure during the surgery [17]. Another major advantage is the reproducibility associated with computer-assisted planning [17]. Despite the strong advantages that computer-assisted planning offers, costs, time, effort, and expertise to generate a 3D-preoperative planning remain too high [18]. Even for simple osteotomies, preoperative planning time can take up to several hours [19]. The result of this is that the clinical application is still limited. The limitation in the ability to fully exploit the clinical benefits of 3D computer-assisted planning indicates the need for an automatic planning method. This method should explore feasible osteotomy approaches and select an optimal plan while reducing the workload for the planning.

Several approaches for automation and/or optimization of 3D computer-assisted preoperative planning of corrective osteotomies have been described in the literature. Different methods are employed depending on the type of bone, the type of deformity, and the goal of the osteotomy. For the forearm specifically, the contralateral bone is most often used as a reconstruction target. If the affected bone is registered to the contralateral bone both proximally and distally, the deformity of the bone becomes visible and can be quantified. To determine the optimal osteotomy plane, different methods have been described, such as minimization of the bone cut surface, or minimization of the bone protrusion. The optimal osteotomy plan is dependent on the anatomic reconstruction goals, which have to be clearly specified. It can be concluded that the emergence of different 3D computer-assisted planning techniques and especially the implementation of automatic optimization techniques can contribute to faster, more accurate patient-specific bone deformity diagnosis and osteotomy planning for malunions of the forearm.

1.1. Aim and objectives

Currently, at the Department of Orthopedics in the Erasmus MC, most cases of forearm malunions that require a corrective osteotomy are planned using computer-assisted planning. These preoperative plannings are made in 3-Matic (Materialise), a design optimization software [20]. Making these plannings is time-consuming, as virtually mimicking all steps of the surgery is done manually. The time investment is especially high because a process of trial-and-error is required to find an optimal plan. It is also desirable to compare multiple scenarios and their outcomes. Time reduction and increased computational power are therefore required, leading to the aim of this research. This research aims to automate the workflow of finding a computer-assisted optimized planning for corrective osteotomies of the forearm. The research question of this thesis is formulated as:

How can the computer-assisted patient-specific corrective osteotomy planning for forearm malunions be automated and optimized?

The contents of this research can be divided into two main objectives.

1.1.1. Objective 1: Automation

The first objective is the automation of the workflow of computer-assisted planning for corrective osteotomies. The purpose of this is to reduce the time that is spent manually performing steps that are routine for each patient. 3-Matic has a scripting module that uses Python API, which lets the user automate their processes to make it faster and more robust.

1.1.2. Objective 2: Optimization

The second part of the research consists of the implementation of an optimization algorithm to calculate an optimal patient-specific osteotomy plan. In this part, many feasible osteotomy plans have to be generated, explored, and evaluated. The evaluation should happen according to the anatomical reconstruction goals for the malunion. Throughout the optimization, new and improved solutions should be generated. Finally, an osteotomy plan will be selected that satisfies the anatomical reconstruction goals of the corrective osteotomy.

1.2. Thesis Outline

This thesis consists of 6 chapters following this introduction. First, in Chapter 2 some relevant background information regarding computer-assisted planning for corrective osteotomies of forearm malunions is given. The anatomy of the forearm and the pathomechanisms of a forearm malunion are explained. Additionally, a general introduction into computer-assisted surgery and basic terminology is given. Finally, the topic of optimization briefly addressed to explain the basic concepts of optimization in general. In Chapter 3, the workflow of planning a corrective osteotomy is explained into more detail. For each step, the methods used to automate the workflow are described. Chapter 4 discusses the anatomical reconstruction goals and the optimization algorithm that is implemented. The optimization is applied to 15 patient cases of forearm malunions. In Chapter 5, the validation method is described. The resulting osteotomy plans from the optimization and the validation results are presented in Chapter 6. Finally, in Chapter 7, the presented work and the results are discussed. Moreover, the clinical relevance of this thesis is addressed. In Chapter 8, the final conclusions of this thesis are given and future recommendations are proposed.

2
Background

In this chapter, some relevant background information on the topic of this research is given. The anatomy of the forearm, malunions of the forearm, computer-assisted reconstructive surgery, and optimization are briefly discussed.

2.1. Anatomy of the forearm

The forearm plays an important role in facilitating the positioning of hand in space and thus helping to provide the upper extremity with mobility [21]. It is a complex functional unit with two bones articulating with each other. To be able to understand functional limitations caused by a malunion, it is important to consider all anatomical structures of the forearm and their interactions. In Figure 2.1, the bony anatomy of the radius and ulna is visualized. In neutral position, the ulna is on the medial side and the radius is located lateral. The radius shape naturally follows a complex angle and curve, with most importantly the lateral curve called the radial bow. This radial bow plays an important role during rotation of the forearm, where the radius rotates around the ulna [3]. The radius and ulna articulate with each other at two joints [22]. The first one is the proximal radioulnar joint (PRUJ), where the head of the radius and the radial notch of the ulna articulate. This joint is stabilized by the annular ligament and elbow joint capsule [3]. Second, the head of the ulna and the ulnar notch of the radius articulate at the distal radioulnar joint (DRUJ). The triangular fibrocartilage complex and the wrist joint capsule primarily stabilize the distal radioulnar joint [3]. Distally, the radius also articulates with the os lunatum and the os scaphoideum at the radiocarpal joint (RCJ) [23]. Proximally, the radius and the ulna articulate with the humerus. The interosseous membrane connects the radius and the ulna and is composed of several ligaments that have an oblique direction [24]. These ligaments ensure forearm stability, and transfer loads from the distal radius to the proximal ulna [24]. Furthermore, the interosseous membrane maintains the interosseous space between the radius and ulna during forearm rotation. The m. biceps brachii, the m. supinator, the m. pronator teres, and the m. pronator quadratus enable pro- and supination, see Figure 2.1. The last three muscles insert into the proximal, middle, and distal thirds of the radius, respectively [9].

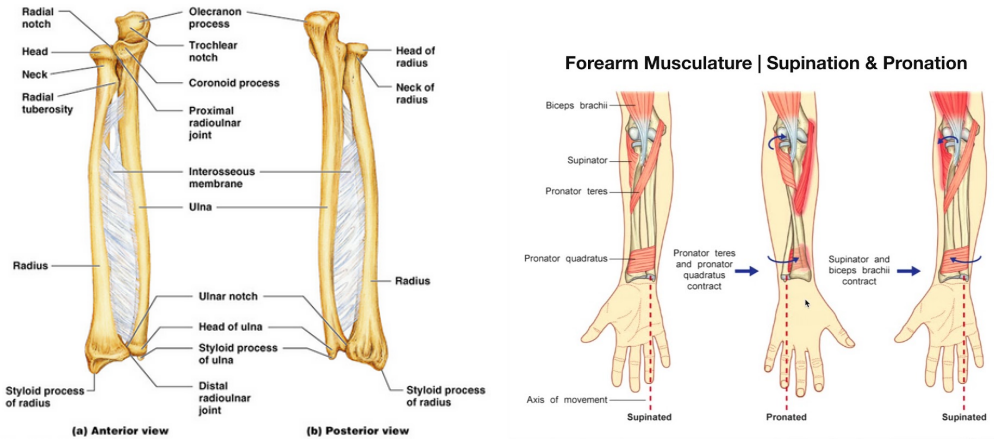

(a) Bony anatomy of radius and ulna [25] (b) Muscles enabling pro- and supination [26]

Figure 2.1: Anatomy of the forearm.

2.2. Malunion of the forearm

Malunions occur when fractures of the bone do not heal properly. The deforming forces exerted by the supinator, pronator teres, and pronator quadratus muscles acting on the fracture fragments can lead to angulation, rotational deformities, or combined deformities [9, 21]. As a result, the bone can be deformed or abnormally positioned. The malunion can be expressed in different deformities of the bone, see Figure 2.2. Malunions of the forearm can lead to limitations in the Range of Motion (RoM) through different mechanisms [27]. Angular deformities can cause tension in the interosseous membrane and bone impingement, leading to restricted radial rotation about the ulna [9, 27]. Angular deformities appear in combinations of different directions: dorso-volar angulation, radio-ulnar angulation,

Table 2.1: Type of angulations caused by malunions of the forearm

Angulation	Deformity	Measured in
Dorso-volar	Extension-flexion	Sagittal plane
Radio-ulnar	Varus-valgus	Coronal plane
Internal	Pronation-supination	Axial plane

and internal angulation. The angulation can be measured on X-ray imaging, but more accurately on CT-imaging. In Table 2.1, an overview of these angular deformities is given and in which plane they can be measured. Axial malunions can cause malalignment of the PRUJ and DRUJ [9, 27]. This can lead to stiffness and limited forearm rotation. Another important aspect of malunions is the shape of the radius bone. A change in the radial bow due to a malunion can also limit rotational movement [28].
Evidently, the degree of angulation, the location of deformity, and one or both forearm bone involvement all play an important role in the limitation in forearm function and thus the clinical consequence of the malunion [9]. Because of the complexity that malunions can exhibit, restoration of the length, axial alignment, rotational alignment, and displacement is required to restore pronation and supination [3]. Moreover, soft tissue and joint-related factors should also be taken into account when assessing the functional limitation causes by a malunion.

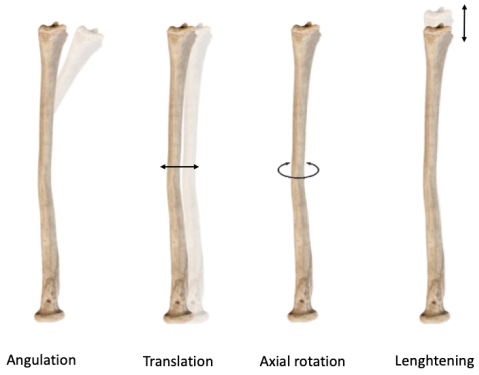

Figure 2.2: Parameters to describe the deformity of a radius.

2.3. Computer-assisted reconstructive surgery

Computer-assisted surgery (CAS) is the concept of using computer technology for surgical planning, and for guiding or performing surgical interventions. In CAS, 3D models of organs or bones are reconstructed from medical imaging modalities. Different modalities can be used for this, with CT being the gold standard for high-accuracy geometric models of the bone [29]. From the segmentation of the bone on CT images, a polygonal mesh is reconstructed using algorithms like the Marching Cubes algorithm. A polygonal mesh defines a surface model and represents the shape of an object. It is a collection of polygons, which are usually triangles, that are made up of vertices, edges, and faces (see Figure 2.3) [1]. Vertices are the corners, edges are the lines between the faces, and the faces are the flat surfaces. The polygonal characteristics of 3D surface models are important because they allow to perform calculations on the bone models. For example, each triangle has a normal vector, representing the direction of the surface at a certain point. Another example is that the coordinates of vertices can be accessed to calculate the distances between or the sizes of bones.

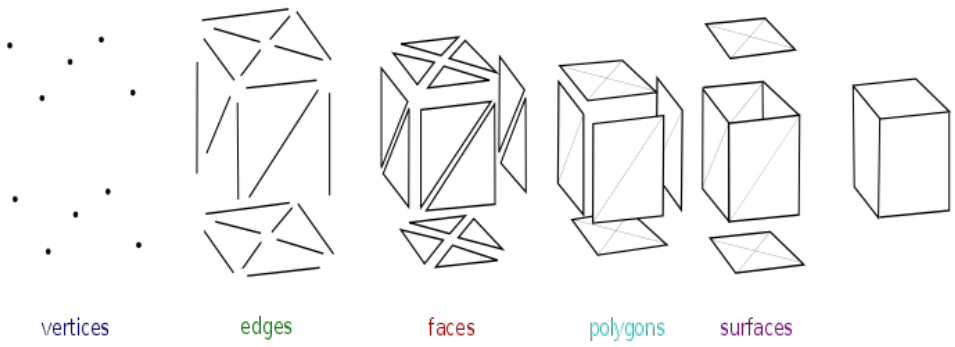

Figure 2.3: Vertices, edges, and faces forming a surface model [1].

For corrective osteotomies of forearm malunions specifically, a bilateral CT scan is acquired. The surgeon is then able to get a 3D insight into the anatomy of the malunion. In particular, the deformed bone can be compared to the healthy, contralateral side to give an idea of what the bone should look like. Based on the 3D models of the bones, the surgery can be mimicked virtually before the physical surgery. A typical computer-assisted planning for a corrective osteotomy of the forearm roughly consists of the following steps, that are visualized in Figure 2.4:

1. Acquisition of bilateral CT-scan
2. Segmentation of bones of interest and reconstruction of 3D surface models
3. Quantification of the deformity of the pathological bone
4. Determination of the position of the osteotomy plane: orientation and location
5. Bone reduction
6. Positioning of the plate and screws
7. Design of patient specific surgery guides

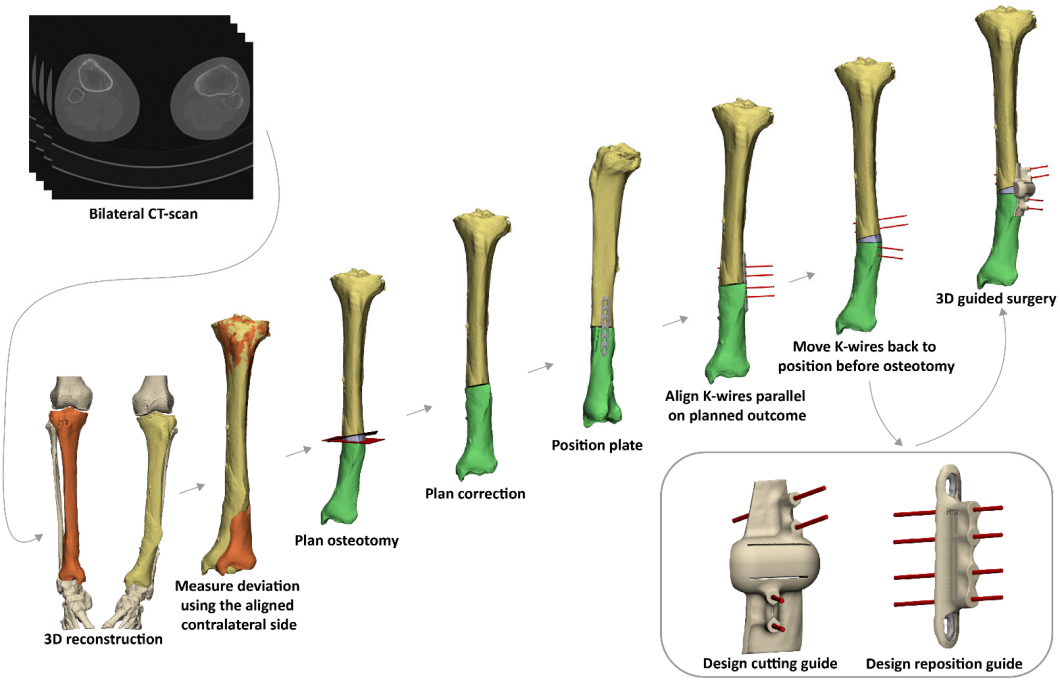

Figure 2.4: A typical computer-assisted corrective osteotomy planning workflow, illustrated for the tibia [2].

2.4. Automation

Automation is the use of technology to program a process to run on its own without or with minimization of human intervention [30]. Simple, repetitive tasks are automated to save time and improve productivity [31]. Programming languages can be used to create software programs, like mobile applications or the interface of manufacturing machines [30]. Python is an example of a programming language and is one of the most widely used languages.

2.5. Optimization

Optimization is the act of making something as good as possible [32]. More specifically, mathematical optimization is the collection of mathematical principles and methods used for solving quantitative problems in many disciplines, including physics, biology, engineering, economics, and business [33]. Four fundamental elements to optimization can be recognized in any optimization problem [33]. The first one is an objective function that is to be maximized or minimized. The second element is a collection of variables of which the values can be manipulated in order to optimize the objective. Thirdly, a set of constraints is always required, which are the restrictions on the values that the variables can take. The constraints on the variables determine the search landscape, which is the space of all feasible solutions [34]. Finally, an algorithm is needed that combines these three elements. Many different optimization algorithms can be used for this. Optimization algorithms aim to find the input parameters or arguments to a function that result in the minimum or maximum output of the function [35].

As for the case of computer-assisted planning of corrective osteotomies, optimization can also be used. The four fundamental elements of optimization can be applied to the aim of this thesis to understand the optimization problem. Optimization of the corrective osteotomy planning is about finding an osteotomy plan that satisfies all anatomical reconstruction goals. The objective function is in this case a combination of the anatomical reconstruction goals of the corrective osteotomy. The variables are the parameters that determine what an osteotomy plan looks like. The constraints are the values of the parameters that would result in an unfeasible osteotomy plan and thus guarantee the output of an optimal plan.

3
Automation

In this chapter, the steps of the developed automatic computer-assisted planning workflow for corrective osteotomies of the radius are described. The aim of this automatic workflow is to align the pathological bone to the mirrored reference bone. This can give the surgeon an insight into the degree and nature of the deformity. For each step, it is explained which methods and algorithms are used. The entire process is visualized in Figure 3.1.

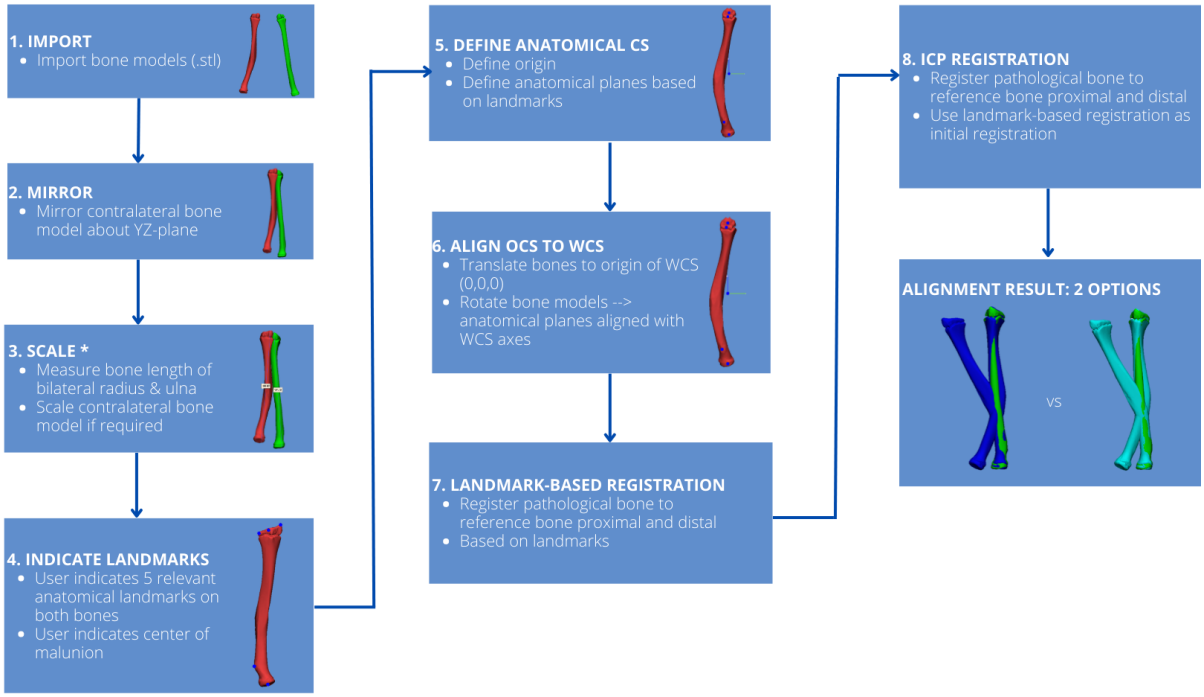

Figure 3.1: The automated workflow of bone model registration. Result is the proximal and distal registered bones, with two options to choose from. ** = optional. Abbreviations: CS = coordinate system, OCS = object coordinate system, WCS = World Coordinate System, ICP = Iterative Closest Point. Color legend: red = pathological bone, green = reference bone, dark blue and light blue = pathological bone registered proximally and distally to reference bone, using two different alignment percentages.*

3.1. Data preparation

In this section, a few steps are described that are required to prepare the models for registration.

3.1.1. Mirroring and scaling

The input of the automatic workflow is the .stl files of the pathological bone and the contralateral bone. These .stl files are retrieved from CT-scan data, where the patient is scanned in prone position with the arm above the head [36]. The CT-scan coordinate system is positioned with the z-axis along the patient table. Therefore, when importing the bone models in 3-Matic, they are oriented with the length of the diaphysis in the direction of the z-axis of the coordinate system. First of all, the contralateral bone will be mirrored about the YZ-plane, using the trimatic function *<Mirror>*. If the CT-scan is made in line with the standard CT-scan protocol, the pathological bone model and the contralateral bone model will then be similarly oriented. The dimensions of the bone models are then measured, to see whether the two bone models differ in length. Possibly, bone shortening or lengthening of the pathological bone has occurred as an effect of the malunion. To compensate for this, scaling is sometimes required to ensure planning towards a representative target. This can be based on the length difference between the ulnae of both sides. The user can indicate whether scaling is desired and if so, the contralateral bone (reference) is scaled using the trimatic

function <*Scale*> with a scaling factor:

$$scaling\ factor = \frac{length_{patbone}}{length_{refbone}} \tag{3.1}$$

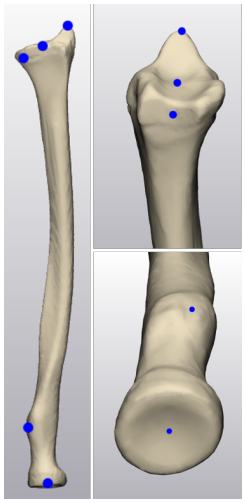

Figure 3.2: Landmarks for the radius (right). *Left: volar view, right top: distal view, right bottom: proximal view.*

3.1.2. Definition of an anatomical coordinate system

When the models are imported into 3-Matic, they are positioned somewhere in space according to their position relative to the CT-scanner coordinate system. It is desirable to place the models at the origin of the coordinate system of the 3-Matic environment, which is the the World Coordinate System (WCS). The WCS is located at the 3D-coordinates (0,0,0) and can not be moved. The translations or rotations that are applied to the bone model in 3-Matic are given relative to the WCS. If the bone models are positioned distant from this WCS, it is harder to intuitively understand the rotations. Besides working with the bone models at the origin of the WCS, the definition of an anatomical coordinate system is relevant. This facilitates the interpretation of the transformations around the x, y, and z-axis as clinically relevant movements. The Standardization and Terminology Committee (STC) of the International Society of Biomechanics propose a general reporting standard for joint kinematics based on the Joint Coordinate System (JCS) [37]. According to this standard, a coordinate system for the radius can be established based on relevant landmarks. In Figure 3.2, these landmarks are visualized. So, the user is asked to indicate the following five landmarks:

1. Point of maximal concavity of the proximal radial head
2. Radial tuberosity
3. Radial styloid
4. The center of the ridge between the radiolunate fossa and the radioscaphoid fossa
5. Sigmoid notch

These landmarks must be indicated on both the pathological bone and the contralateral bone correspondingly. With these landmarks, the anatomical axes can be determined. The origin of the radial coordinate system is placed halfway between the center of depression of the proximal radial head (point 1) and the center of the ridge between the radiolunate fossa and the radioscapoid fossa (point 4). The long bone axis is also defined between these two points. A rotation of the radius around this axis signifies pronation and supination. The second axis is perpendicular to the long bone axis, and lies in the plane between the radial styloid (point 3), the sigmoid notch (point 5), and the origin. This is the medial-lateral plane. Finally, the third axis is in the plane perpendicular to the first two axes. Movements in this plane are in the volar-dorsal direction. In Figure 3.1 (step 5), the anatomical coordinate system for the radius is visualized.
After the anatomical coordinate system is defined, the bone models can be placed at the origin of the WCS. The anatomical coordinate system will be aligned with the WCS. By doing so, a rotation around a certain WCS axis corresponds to a clinically relevant movement. With the trimatic function <*Change OCS to WCS*>, the contralateral radius is placed at the origin of the WCS and the anatomical coordinate system is aligned with the WCS. The same translation is applied to the pathological bone, so that it is moved along with the reference bone to the WCS origin.

3.2. Landmarks-based initial registration

After aligning the anatomical coordinate system with the WCS, the pathological bone can be registered to the reference bone. A registration algorithm will be used for this that aims to find the transformation between a point cloud and some reference surface [38]. Registration algorithms rely on a rough initial estimation of the registration [39]. To do so, a landmark-based registration is performed prior to the registration. For this, the trimatic function *<N-points registration>* is used, with the corresponding landmarks on the pathological and reference bone as indicated in Section 3.1. The model is registered separately on the proximal and distal end. For the proximal landmark-based registration, the center of depression of the proximal radial head and the radial tuberosity are used. For the distal landmark-based registration, the radial styloid, the center of the ridge between the radiolunate fossa and the radioscaphoid fossa, and the sigmoid notch are used.

3.3. Iterative Closest Point Registration

After the landmark-based registration, the registration can be applied. An Iterative Closest Point algorithm is used for this. ICP tries to find the closest point pairs and iterates until the point matching error stabilizes [40]. The ICP registration is also performed separately for the proximal and distal ends of the bone. The trimatic function *<Global Registration>* is used to this end. This function works specifically on triangle nodes of the meshes. By minimizing the node-to-node distance, the bone models will be registered on each other. The function has three parameters that have to be set by the user: the subsample percentage, the distance, and the number of iterations. The subsample percentage holds the subset of the nodes from the bone models that will be considered during each iteration. The Average Distance Error is calculated between the subset of nodes of the two bone models and is iteratively minimized. For setting this parameter, a trade-off must be made between computational time and power and detail. A higher subsample percentage will lead to a more accurate registration, but will be more time-consuming due to the computational power required. The distance parameter determines the search radius the algorithm uses to find the closest corresponding node on the other bone model. If the distance threshold is set to a low value, the algorithm might get stuck in a local minimum. This means that the algorithm will find a registration result close to the current one because the algorithm does not search for nodes that are further away. The registration result will therefore be sub optimal. If the distance parameter is set to a high value, the ICP will try to minimize the error in a wider range. This leads the ICP to attempt registering the bone models also where they deviate, compromising its ability to accurately register the proximal or distal part. However, once the algorithm gets close to an accurate registration between the two bone models, the distance threshold must be lowered, to also find smaller improvements. The number of iterations parameter again must be balanced between time and detail. A higher number of iterations will lead to a more accurate registration result but will take up more time. In Table 3.1, an overview is given of the values that are used for each parameter throughout multiple runs.

Table 3.1: Global registration settings for run 1, 2, and 3

	Distance threshold	**Subsample %**	**Number of iterations**
Run 1	20	35	200
Run 2	Automatic	35	200
Run 3	Automatic	35	200

The registration of the bone models is not performed on the full length of the bone models, but only on proximal and distal segments. This is to exclude the deformity from the registration and to ensure accurate registration of the joints. To determine the segment of the bone that is used for alignment, the user is asked to indicate the center of the malunion. Based on the location of the malunion along the long bone axis, the proximal and distal alignment percentages are determined. In Figure 3.3, the boundaries for the distal and proximal alignment parts are visualized. The alignment percentages are calculated as follows:

$$alignment\ percentage = \begin{cases} \frac{height_{malunion}}{length_{patbone}} - 0.1 & \text{for proximal alignment} \\ \frac{height_{malunion}}{length_{patbone}} + 0.1 & \text{for distal alignment} \end{cases} \tag{3.2}$$

Since this registration percentage has an impact on the result of the alignment, an alternative alignment is calculated as 10% smaller than the first alignment percentage. The smaller the alignment percentage, the more accurate the alignment will be at the proximal or distal extremity of the bone models. This is because a smaller alignment percentage will allow the ICP to focus on a smaller part of the bone models to register. However, this will also result in the pathological bone model starting to deviate from the contralateral bone model earlier along the long bone axis. Thus, the two alignment percentages allow the user to compare the registration result, and make a trade-off between overall alignment and joint alignment. The choice of the best alignment percentage is left to the user. This is because other factors like the clinical picture that the patient presents with, can play a role in deciding how precise the joint surfaces need to be aligned.

3.4. Registration result

The proximal and distal registered bone models give an insight into the degree of deformation, see Figure 3.4. By visualizing the proximal aligned pathological bone model to the contralateral bone model, it can be clearly distinguished where the pathological bone starts to deviate from the reference bone along the long bone axis. By comparing the distal joint surface of the pathological and contralateral bone models, the nature of the deformity can be interpreted. It can be distinguished whether the malunion is purely angular, or whether a rotational component is also present. By simultaneously visualizing the proximal and distal registered bone in comparison to the reference bone, the region of deformation can be identified. This is also an indication of the range along the bone axis where the osteotomy cut can be placed.

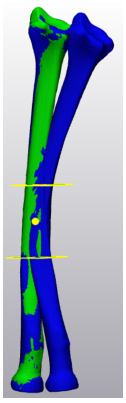

Figure 3.3: Parts used for alignment. *Yellow point = center of malunion, yellow planes = boundaries used for alignment of proximal and distal part. Blue = pathological bone proximally and distally registered, green = reference bone.*

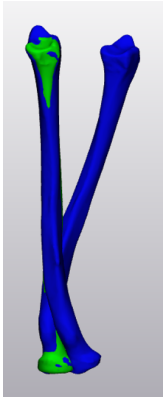

Figure 3.4: Region of deformity becomes visible after alignment. *Blue = pathological bone proximally and distally registered, green = reference bone.*

4 Optimization

After the bone models have been registered, the bone correction can be planned. The aim of the correction osteotomy is to restore the function of the forearm. To do so, an osteotomy plan has to be determined that optimally satisfies the anatomical reconstruction goals. To create such a plan, different plans have to be generated, compared, and improved based on evaluation. To this end, an optimization algorithm is implemented. This allows to automatically develop a set of solutions, evaluate the resulting bone correction, and improve towards an optimal osteotomy plan. As stated in Section 2.5, optimization knows four fundamental elements. In the following sections, these different aspects of the optimization process will be discussed. Section 4.1 will discuss the optimization algorithm that is implemented and the general construction of it. In Section 4.2, the objective function that is used for the optimization is explained, supported by the anatomical reconstruction goals. Based on the implemented algorithm, the structure of the variables and constraints are discussed in Section 4.3 and Section 4.4 respectively. In the sections thereafter, some additional operators specific to the implemented optimization algorithm are explained for this research specifically. Finally, in Section 4.10, the general outline of the implemented algorithm is explained providing pseudocode.

4.1. Optimization algorithm

For the optimization, an Evolutionary Algorithm (EA) is implemented. EAs are heuristic stochastic direct search algorithms, meaning that they are based on trial-and-error and include random variables. It is a type of algorithms that perform optimization with the ability to evolve [41]. EAs are inspired by biological evolution and natural selection. The basic idea behind EAs is the generation of a population of candidate solutions and iteratively improving them through a process of selection, reproduction, and mutation. Only the fittest solutions are selected and passed on to the next generation, whereas the unfit solutions will be removed from the population throughout the generations. Thus, EAs are trying to reach optimal states by successive improvements [42]. EAs are well-suited to optimize problems with multiple objectives and non-linear constraints, which is the case for corrective osteotomies. Another advantage is that they are able to handle problems with a large number of variables. Even in complex optimization problems with a large number of variables, EAs can significantly speed up the process. This is due to the parallel characteristic of EAs. Maybe most important is the feature of being able to find multiple local optima in a complex search space, as opposed to for example downhill simplex optimizers. This is because EAs can manage the trade-off between exploring the entire search space and fully exploiting the current solutions [43]. All before mentioned characteristics are not only beneficial to the nature of the optimization problem proposed in this thesis, they also allow further expansion of the optimization in the future.
Evolutionary Algorithms have three main characteristics [41]:

- *Population-based*: EAs maintain a set of solutions to optimize the problem in a parallel way.
- *Fitness-oriented*: Every individual has a fitness value, which is an evaluation of the performance. This is essentially the objective function of the optimization problem.
- *Variation-driven*: Throughout the generations of the optimization, the individuals will undergo a number of variation operations. This part of the EAs is fundamental to searching the solution space.

EAs consist of four overall steps: initialization, selection, genetic operators called crossover and mutation, and termination. In Figure 4.1, standard iteration of an EA is visualized [44]. During initialization, an initial set of solutions is generated. This is the so-called population [45]. One solution is called a chromosome or an individual and entails a set of genes. The genes encode the values for the variables that have to be optimized. The initial population is created randomly within the constraints that are set. Each chromosome in the population must be evaluated according to the fitness function. The fittest chromosomes are selected based on this fitness function. After the selection, the genetic operators are applied to the population. In this step, current chromosomes are used to create the next generation in the algorithm [44]. Two main genetic operators are used: crossover and mutation. During crossover, different solutions are combined to create a mixture of the parents' qualities. During mutation, new genetic material is introduced. Both operators are probabilistic, meaning that they occur depending on a certain chance. One run through these steps, which is one circle in Figure 4.1, is called a generation. The algorithm will keep running as long as the stop criterium has not been reached. This can be either a maximum number of generations, or a threshold of performance [44].

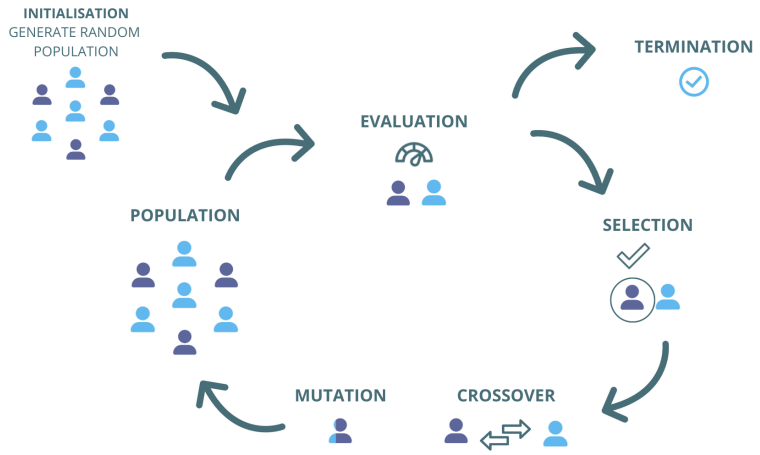

Figure 4.1: The structure of an Evolutionary Algorithm.

4.2. Anatomic reconstruction goals and objective function

Evolutionary algorithms progress based on fitness functions, which are the objective functions as described in Section 2.5. Fitness functions are functions that have to be minimized or maximized in order to find an optimal solution. They represent the quality of a candidate solution, in terms of a certain goal of the corrective osteotomy. These fitness functions can all be combined into one function that assigns an objective score to each candidate solution. The scores can each be given a certain weight factor according to their importance during the optimization. In the case of EAs, this score determines the likelihood that a chromosome survives into the next generation [46]. The better the fitness score, the higher the chance a chromosome will be passed on to a next generation.

To formulate fitness functions, the anatomical reconstruction goals for the corrective osteotomy have to be clearly defined. These goals can then be translated into mathematical expressions. The main motive for doing the corrective osteotomy is restoration of the function of the forearm. For the scope of this thesis, it is assumed that a geometrical restoration of the anatomy of the forearm will result in complete function. As described in Chapter 2, the function of the forearm can be limited due to a malunion through different mechanisms. In this section, these disrupted mechanisms are translated into anatomical reconstruction goals for the corrective osteotomy. The supporting fitness functions are defined and justified.

4.2.1. Anatomic reconstruction goal 1: Distal radial joint surface alignment

As clarified in Section 2.2, malalignment of the joints can cause a rotational limitation in the forearm function. To restore the function of the forearm, an important aspect is aligning the joint surfaces of the radius to the joint surfaces of the mirrored contralateral radius. In Chapter 3, the radius bone models have been proximally registered. This is the input for the optimization process. From this situation, it is assumed that the proximal radial joint surface is well aligned. The first and most important anatomical reconstruction goal can therefore be stated as the alignment of the distal radial joint surface. It is assumed that the alignment of the joint surfaces will result in a functional distal radial joint surface, contributing to a normal forearm function. This goal can be objectified as the minimization of the distance error between the pathological and the reference bone. As the focus is on the distal radial joint surface, this alignment error is calculated between the distal 10% of the pathological radius and the contralateral radius. The Root Mean Squared Error (RMSE) is a commonly used measure for the Euclidean distance in a multidimensional space [47]. So, the fitness function for the distal radial joint surface alignment is given below:

$$RMSE_{alignment} = \sqrt{\frac{1}{n}\sum_{i=1}^{n}(r_i - p_i)^2} \tag{4.1}$$

In this function, *r* are the points of the reference bone and *p* are the points of the pathological bone. In trimatic, the trimatic function *<Part Comparison>* is used to this end. The distal 10% of the pathological and contralateral radius are used as the input for this function. From the retrieved part analysis, the RMSE can be acquired.

4.2.2. Anatomic reconstruction goal 2: Minimization of bone protrusion

Apart from the alignment of the joints, proper function of the forearm is also dependent on a normal shape of the radius and ulna. As described in Section 2.1, the radius has a natural bow that is important for the pronation and supination. If the shape of the radius deviates from this natural radial bow extensively, the function of the forearm

might be lacking, despite of the well aligned joints. This can be caused by two things [48]. On the one hand, an increase in the distance between the radius and ulna can lead to contracture of the central band. On the other hand, a decrease in this distance can lead to bone impingement. Thus, the second anatomical reconstruction goal is restoring the shape of the radius. This can be interpreted as minimizing the deviation of the pathological bone after reduction as compared to the contralateral bone. A part of this is minimizing the bone protrusion. Bone protrusion is the parts of the bone that deviate from the anatomical target and that entail a surface gap among the fragments [14]. The bone protrusion must be minimized around the location of the osteotomy cut, as it impedes the fixation of the osteosynthesis plate and may cause problems with soft tissue surrounding the bone. The location and orientation of the osteotomy plane influence the degree of bone protrusion. The relationship between the osteotomy plane and the degree of bone protrusion is advantageous for the optimization, as minimization of the bone protrusion will be able to control the location and orientation of the osteotomy plane.
Essentially, the bone protrusion can be considered as the RMSE calculation between the reduced pathological bone parts and the reference bone parts around the osteotomy plane. To achieve this, a window function is used. Window functions are functions that analyze the range of data near a given point. The given point in this case is the osteotomy plane with a certain location and orientation. In Figure 4.2, the calculation of the bone protrusion is illustrated. The RMSE between the bone parts is calculated within a given range of the osteotomy plane. To this end, the trimatic function *<Part Comparison>* is used to retrieve the RMSE between the bone fragments. Mathematically, the bone protrusion can be described by [14]:

$$BP(F,R) = \frac{1}{F}\sqrt{\sum W(pl)^2 - \delta(W(pl,p_i),W(pl,R))^2} \tag{4.2}$$

In this function, *F* is the point set of a bone fragment and *R* is the point set of the reference bone fragment. *W* is the window function as a function of the osteotomy plane with a certain location and orientation. The thickness of the window function can be adjusted by the user, but is set to a default of 8 points on the centerline curve. The window thickness is measured in points on the centerline of the bone part. The bone protrusion is calculated for the proximal and distal reduced part of the pathological bone as compared to the contralateral bone. The function for the total bone protrusion is given by [14]:

$$Bone\ Protrusion\ Total = BP(p_{prox},R) + BP(p_{dist,reduced},R) \tag{4.3}$$

It should be noted that the bone protrusion does not account for differences in the diameter of the two bone models. This can introduce a large bias in the measure of bone protrusion in the case that the osteotomy plane is located somewhere in the malunion. The diameter at the site of the malunion is presumably larger than at the same location on the reference bone, due to the rebuilding capacities of the bone after a fracture. This would result in a large bone protrusion at the site of the malunion, introducing a negative bias. To avoid this, the diameters of the pathological and reference bone models are calculated. The total bone protrusion score Equation 4.3 is therefore corrected for the ratio in bone diameters at the osteotomy plane location as following:

$$Bone\ Protrusion\ Corrected = (BP(p_{prox},R) + BP(p_{dist,reduced},R)) * \frac{diameter_{refbone}}{diameter_{patbone}} \tag{4.4}$$

4.2.3. Objective function

As discussed in Subsection 4.2.1, the main anatomic reconstruction goal is the distal radial joint surface alignment. To guarantee this, in this research it is chosen to align the distal 25% of the pathological bone after the osteotomy cut to the distal 25% of the reference bone. The associated benefit of this is that the optimization problem becomes simplified. This is because the variables that would be required for the rotation and translation of the distal part relative to the proximal part after the osteotomy cut become redundant, as the emphasis is now placed on the distal radial joint surface alignment. Thus, the objective function for the optimization can be confined to the minimization of the bone protrusion near the osteotomy plane as described in Subsection 4.2.2. However, a trade-off between distal radial joint surface alignment and restoration of the radial bow must be considered. This will be further explained in Section 4.11.

4.3. Optimization variables

To initialize the optimization algorithm, an initial random population has to be generated. The population size $n_{population}$ can be set by the user, with a default to 26. This number is chosen to balance between computational time and genetic variety, based on trial-and-error. This can be explained as follows: a large population size will allow for more genetic variation, as more genes can be present. However, the larger the population size, the higher the computational time. Each chromosome holds 4 genes that have to be optimized: the osteotomy plane location (z-axis) and the osteotomy plane orientation (x-, y-, and z-axis). In Subsection 4.3.2 and Subsection 4.3.3, the variables for the plane location and plane orientation will be discussed in more detail.

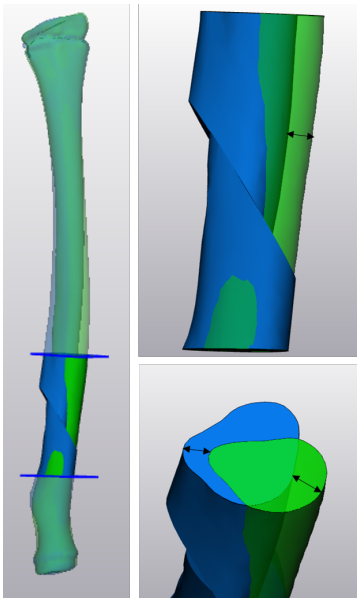

Figure 4.2: Calculation of bone protrusion. *Left: window function used. Right: black arrows illustrate areas with bone protrusion. Green: reference bone, blue: pathological bone after reduction.*

4.3.1. Quasi-random sequence generator

The generation of the initial population is random. This means that a number of chromosomes are randomly sampled with values somewhere in the search landscape, which is bounded by the gene-specific constraints. It has been shown that the initial population has an impact on the final result of the optimization [49]. When using pseudo-random number generators, in theory all chromosomes could be agglomerated in one part of the search landscape. This means that an entire part of the search landscape is not properly explored and thus has a disadvantage. Usually, it is more important that the sample points are as evenly distributed as possible than that they imitate random points [49]. Quasi-random sequences are designed to tackle this problem and have a good uniform distribution. As they fill the hyper-space in an equidistributed fashion, the optimization hyper-space is explored more effectively [50]. The Halton sequence is an example of such a quasi-random sequence generator and is applied in this research for the generation of the initial population [51]. The result of this is that the initial population is generated with gene values that cover the entire search landscape.

4.3.2. Osteotomy plane location

The first gene is the location of the osteotomy plane. In this research, the location is only optimized along the long bone axis (z-axis). A difference in the x- and y- direction does not have an impact on the osteotomy cut, making it redundant. To quantify the location along the long bone axis, a centerline curve is fitted through the bone model using the trimatic function *<Fit Centerline Curve>*. Essentially, this centerline curve can be described as a set of points that are each at the center of axial cross-sections of the bone. From the Halton sequence, each chromosome has an osteotomy plane location appointed somewhere on this curve. The osteotomy plane is then created by using the function *<Create midplane>*.

4.3.3. Osteotomy plane orientation

The orientation of the osteotomy plane can be divided into three genes: namely the orientation relative to the x-, y-, and z-axis. The Halton sequence generates rotation angles for each direction. Using the trimatic function *<Rotate around axes>*, the plane that is created in Subsection 4.3.2 is rotated around the x-, y-, and z-axis. This yields an osteotomy plane with a certain orientation.

4.4. Constraints

Constraints are hard limits placed on the value of the genes [52]. In this research, they are used to prevent the algorithm from finding gene values that will result in unfeasible osteotomy plan solutions.

4.4.1. Constraints on osteotomy plane location

The malunion is most abundant at the site of the initial fracture, making this an obvious location for the osteotomy cut [53]. However, often the malunion covers a range of the bone and more than one exact site could be feasible. Therefore, in this research, the search range for the osteotomy plane location is constrained to a range near the center of the malunion. This is done to prevent the algorithm from looking for osteotomy sites near or through the articular surfaces, while the deformity is most prominent at the malunion. Moreover, cuts through the articular surface

should be avoided. An additional advantage is that it reduces computational time. The plane location boundaries are defined as following:

$$plane\ boundary = \begin{cases} center_{malunion} + \alpha * length_{centerline\ curve}, & \text{for } boundary_{dist} \\ center_{malunion} - \alpha * length_{centerline\ curve}, & \text{for } boundary_{prox} \end{cases} \quad (4.5)$$

α can be set by the user, and has a default to 0.1.

4.4.2. Constraints on osteotomy plane orientation

The orientation of the osteotomy plane also has to be constrained. Extremely steep osteotomies are clinically not feasible, as they would cleave the ends [53]. Moreover, it can result in a discontinuous bone contour. This is undesirable for the soft tissues like muscles surrounding the bone and also for the fixation of the osteosynthesis plate. Therefore, the rotation that is applied to the osteotomy plane for each axis, is constrained to a user-set value, with a default to 45 degrees. Through trial-and-error it was observed that higher values can lead to osteotomy planes that are almost parallel to the long bone axis.

4.5. Selection

In each generation, the fittest chromosomes must be selected from the population to pass them on to the next generation. In this study, k-way tournament selection is employed, as can be seen in Figure 4.3. In this selection method, *k* chromosomes are randomly drawn from the population, and a tournament is held between them. Only the fittest chromosome is selected and is passed on to the next generation [54]. This process is performed multiple times, equal to the size of the population. *k* determines the selection pressure, and therefore the convergence rate [55]. A larger *k* will result in faster convergence, as the weak chromosomes will be easily removed from the population. A smaller *k* on the other hand will keep the diversity in the population, and will thus lead to a slower convergence rate. The selection pressure k_{sp} can be easily adjusted, but is set to a default of 5. This selection method is chosen because it has several advantages, like low vulnerability to takeover by dominant individuals, and less time complexity [56].

4.6. Crossover

One of the main recombination operators in genetic algorithms is crossover. After selection, the current population of chromosomes is paired. During crossover, a pair of solutions is taken (now called parent solutions) and recombined to create new offspring solutions. The offspring inherits some of the good qualities of the parents while also introducing some new, potentially beneficial qualities. Crossover is based on the idea that the exchange of information between two good chromosomes can create even better offspring [57]. In this research, uniform crossover is applied. This type of crossover works generates offspring gene-per-gene. For each gene, it is randomly selected from which of the two parents it inherits the gene values. The ratio is 50-50, which means that for each gene, the chances are equal that the gene is selected from either parent. It should be noted that the osteotomy plane orientation actually consists of three genes. However, during crossover they are considered as one unit. This is because the orientation of the osteotomy plane is dependent on the orientation relative to the x-, y-, and z-axis. If the crossover would be for the x-, y-, and z-axis separately, a whole new plane orientation would occur. However, this is not the purpose of crossover.

A parameter that has to be tuned for crossover is the crossover rate ($r_{crossover}$). This rate determines the chance that a pair of chromosomes undergoes crossover. Typical crossover rates are between 0.6 and 0.95 [58]. In general, a higher crossover probability can lead to a faster convergence on a solution. On the other side, this can result in a loss of diversity in the population [59]. For this research, a default of 0.8 was set for the crossover rate.

4.7. Mutation

The final step in the optimization process is mutation. This technique is used to maintain diversity in the population throughout the generations and to avoid getting stuck in local minima [59]. During mutation, the values of all genes of the parent chromosome are cloned to an offspring chromosome. For each gene, it is then randomly decided whether mutation occurs. A parameter called the mutation rate ($r_{mutation}$) or the mutation probability determines the likelihood that a chromosome will undergo mutation. Mutation rates are often described between 0.001 and 0.01. Also common is to set the mutation rate to:

$$r_{mutation} = \frac{1}{number\ of\ genes} \quad (4.6)$$

However, only 4 genes are used in this research, which would result in a mutation rate of 0.25. A high mutation rate can cause the loss of good solutions, while a too small mutation rate can lead to the loss of genetic variation. Therefore, a balance has to be found that lets the algorithm explore the search space while also keeping the good

solutions. Therefore, the mutation rate in this research is set to a default of 0.15. Different types of mutation can be employed, depending on the problem and the type of genes. The mutation algorithm that is used in this study is the Random Resetting Mutation [60]. In this type of mutation, the selected gene value is replaced by a random value within the allowed gene-specific range.

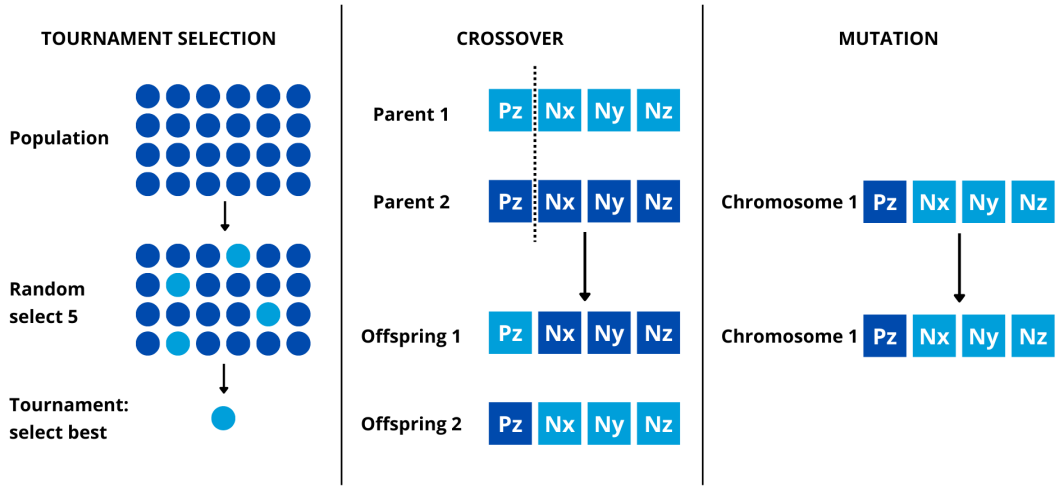

Figure 4.3: Selection, crossover and mutation in EA. *Pz = plane position along z-axis, Nx, Ny, Nz = plane orientation relative to x-,y-, and z-axis.*

4.8. Randomness

Throughout the algorithm, the goal is to minimize the objective function to get closer to an optimal solution. The chromosomes in the initial population and in the populations during the first few generations are presumably quite random and their scores might be sub-optimal. Therefore, new random solutions could improve the score of the solutions by searching other parts of the search landscape. After multiple generations, the solutions in the population are getting closer to an optimum. Then, when mutation occurs, it is desirable to pick values from a range closer to the current solution instead of letting the algorithm pick a value that is very far away from the current value. Therefore, the randomness of mutation is adjusted throughout the generations. While the score is still larger than a predefined value, the mutation value can be chosen from the entire gene-specific range of values. This is to allow searching the entire landscape. When the score drops below a second predefined value, the range is adjusted. Mutation can now only occur within a range around the current solution. The mutation value is then drawn from a normal distribution. This distribution is centered around the current gene value (mean of the distribution), and has a standard deviation that can be set by the user. Finally, when the score becomes smaller than the third predefined value, the standard deviation of the normal distribution is set even smaller around the current solution.

4.9. Elitism

Mutation and crossover occur randomly and change the gene values of the chromosomes. Like in evolution, genetic drift can occur. Genetic drift is the change in frequency of an existing gene variant in the population due to random chance. Due to the stochastic nature of the selection tournament, the population can converge to single solutions [61]. Gene variants can disappear completely, while other gene variants can become fixed. Genetic drift is unguided, meaning that the fittest chromosomes are equally subject to the effects of genetic drift as the weakest [62]. Moreover, the balance between exploration and exploitation is often lost in runs of EAs [63]. To alleviate the before mentioned problems of EAs, elitism schemes can be applied. In elitism, the fittest chromosomes are automatically passed on to the next generation, unaltered. This is achieved by ranking the chromosomes based on their total fitness score. Only the *n* fittest individuals are selected and are guaranteed a place in the next generation, without undergoing crossover and mutation. The user can set the n_{elites} and it is set to a default of 5 in this research.

4.10. Outline of the optimization

Prior to the optimization, an initial random population $n_{pop} = 24$ is generated. The proximal aligned pathological bone will be cut with a plane with the location and orientation as retrieved from the chromosomes in this population. The distal parts after the cut will be registered to the reference bone based on the distal 25%. This is done using the trimatic function *<Global Registration>*. The distance threshold for the first run of the registration is determined by the current distance between the distal parts of the pathological bone and the reference bone, see Figure 4.4. This distance is calculated between the radial styloid of both bones, and is rounded up to the nearest 10 mm. The registration is run until the residual error is smaller than 0.005 between three subsequent runs. All settings for the

runs of the registration can be found in Table 4.1.

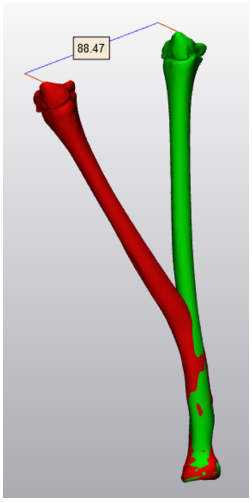

Figure 4.4: Distance measurement between radial styloid landmarks. *Red: pathological bone, green: reference bone.*

When the optimization is initiated, the scores of the population are determined by calculating the bone protrusion, see Subsection 4.2.2. Then, a tournament selection is held to select chromosomes. The selected chromosomes are then paired to become "parents". Each pair creates two offspring chromosomes by cloning the parent chromosomes. These offspring chromosomes might undergo recombination operators, depending on the $r_{crossover}$ and $r_{mutation}$. This is determined by drawing a random number between 0 and 1. If this number is smaller than $r_{crossover}$, the two offspring chromosomes will undergo crossover. Another random number is drawn to determine whether mutation occurs, following the same principle. Resulting from this is the new generation of chromosomes. This new generation of chromosomes has different combinations of osteotomy plane locations and orientations. With these new osteotomy planes, the proximal aligned pathological bone can be cut and registered to the reference bone again. Hereafter, the process starts from the beginning again, following all subsequent steps explained in this section. However, from the second generation on, elitism will also be applied. Because of this, fewer chromosomes are selected in the tournament, namely $n_{pop} - n_{elites}$. The n_{elites} fittest chromosomes are kept separately, and passed on to the next generation without undergoing crossover or mutation. All other steps will be performed as described above. This process continues until the maximum number of generations n_{iter} has been reached. In algorithm Algorithm 1, the pseudocode of the optimization algorithm is given.

Table 4.1: Global registration settings for *run 1...i.* RS = radial styloid

	Distance threshold	**Subsample %**	**Number of iterations**
Run i = 1	$\delta(RS_{patbone}, RS_{refbone})$	35	20
Run i = 2	10	35	20
While i < 8 and $error_i - error_{i-2} > 0.005$	Automatic	35	20

4.11. Final alignment

The optimization results in an optimal osteotomy plane location and orientation. Throughout the optimization, the most distal 25% of the bone is used for the Global Registration. The optimization is driven towards minimal bone protrusion near the osteotomy plane and guarantees alignment of the distal radial joint surface. However, as discussed in Subsection 4.2.2, the shape of the entire radius is important for the function of the forearm. To account for this, it is interesting to experiment with different distal alignment percentages. A smaller alignment percentage means that there is more focus on the distal radial joint surface and will therefore result in a more precise alignment of the distal radial joint surface. However, the overall alignment of the radius shape might deviate more. On the other hand, a larger alignment percentage will focus on the entire distal part of the radius after the osteotomy cut for alignment, resulting in an overall better shape of the radius and thus restoration of the radial bow. This might decrease the accuracy of alignment of the distal radial joint surface slightly. From this, it can be concluded that a trade-off has to be found between the distal radial joint surface alignment and the overall radius shape restoration. This trade-off can be found by varying the distal alignment percentage. Thus, after the optimization has been run, two scenarios are added to the osteotomy plan. One with an alignment of only the most distal 15%, and one with an alignment using the entire distal part after the osteotomy cut (named 100% hereafter). As this trade-off often depends on personal patient factors and patient-specific anatomic reconstruction goals for the osteotomy,

the surgeon can choose between the three scenarios (15, 25 or 100%). The user can assess which alignment percentage will yield the best result for the patient specifically. One important comment has to made regarding this. If the malunion is located very distal, comparing the three scenarios will probably result in only very small differences. Accordingly, comparing the three scenarios is not very useful.

Algorithm 1 Optimization of osteotomy plan

Input: Initial population, proximal aligned bone cut with planes with values from chromosomes
Output: Optimal osteotomy plane location and orientation

$generation \leftarrow 0$
while $generation < n_{iter}$ **do**
  calculate bone protrusion
  keep n_{elites} best chromosomes apart
  perform tournament selection until $(n_{pop} - n_{elites})$ chromosomes selected
  pair chromosomes
  for pair **in** population **do**
    $offspring \leftarrow$ cloned pair
    draw random number *R* in (0,1)
    apply crossover if *R* < r_{cross}
    for chromosome **in** offspring **do**
      apply mutation **if** *R* < $r_{mutation}$
    end for
  end for
  $offspring \leftarrow offspring + elites$
  cut pathbone$_{aligned,prox}$ with planes from offspring
  Global Registration of pathbone$_{dist}$ to refbone
  $population \leftarrow offspring$
  $generation \leftarrow generation + 1$
end while

5 Validation

The validation of the implemented optimization consists of two parts. 15 patient cases with preoperative and planned data are available, which have all been planned by Materialise. These cases will serve as a standard for comparison, because all plannings have been accepted and performed. The first part of the validation consists of a comparison of residual alignment errors between the planned osteotomy and the osteotomy plan resulting from the optimization. Although these scores are objective, a better score does not necessarily imply a better osteotomy plan. This is because these scores are dependent on the characteristics of the malunion and do not include soft tissue anatomy and plate positioning feasibility. Therefore, for the second part of the validation, the results of the optimization were presented to dr. J.W. Colaris, orthopedic surgeon at the Erasmus MC. Finally, the repeatability of the optimization was analyzed as described in Section 5.3.

5.1. Residual alignment errors

The most objective method to validate the optimization is to compare the residual alignment error of the planning$_{automatic}$ for each patient case with that of the planning$_{manual}$. To this end, the residual error between the pathological bone after the osteotomy cut and the reference bone can be calculated for the planning$_{automatic}$ and the planning$_{manual}$ for each patient case. To determine the residual alignment error, the RMSE was acquired. In line with the anatomic reconstruction goals, the residual alignment error was calculated for the entire bone and for the distal 10% specifically. This is done to be able to analyze the entire shape of the radius but also the distal joint surface specifically.

5.2. Qualitative scores

The residual alignment errors as calculated in Section 5.1 serve as a means of objective comparison. For the second part of the validation, dr. J. W. Colaris (orthopedic surgeon, highly experienced in performing this type of corrective osoteotomies) was asked to score the osteotomy plans of both the planning$_{automatic}$ and the planning$_{manual}$. The purpose of this was to compare feasibility scores based on experience and knowledge regarding the approach, the plate positioning, soft tissue involvement and the bone overlap. This score is more relevant from a clinical point-of-view because it is more comprehensive. To this end, dr. Colaris was blinded to the planning method. This was achieved by assigning random case numbers to each osteotomy planning. Dr. Colaris was asked to score each planning between 6 and 10. If the score was to be below 6, the planning was scored as unfeasible. Moreover, an explanation for the score was noted because it is relevant to know in which aspect the planning is lacking for future improvements.

5.3. Repeatability

Not only the quality of the results of the optimization are interesting, the repeatability of the algorithm in generating osteotomy plans is important. Repeatability measures the consistency of a measure from one time to another [64]. Applied to this research, repeatability is the consistency of the generated osteotomy plans if the optimization is run multiple times for the same patient case. Although this is hard to determine due to the stochastic nature of the EA, this measure is important for determining the applicability of the optimization. It would be acceptable if the algorithm results in different plans when it is run multiple times for the same patient case. However, the quality of these plans should be similar and not dependent on the run. If the results of the optimization are not consistent in their quality, the use of the optimization is still not clinically feasible. To investigate the repeatability of the algorithm, the algorithm was run an additional time for the one patient case. Due to limited time, it was not possible to run the algorithm multiple times for each patient.

6
Results

In this section, the outcomes of the optimization are presented and compared with the osteotomies for each patient case as planned by Materialise. To get an idea of the degree of deformity, the transformation matrix between the proximal aligned bone and the reference bone was obtained. This matrix holds the rotation around and translation along the axes. In Appendix A, the Euler angles retrieved from the transformation matrix are displayed for each patient case in Table A.1.

The optimization process could be run without errors for all patient cases except for case 13. This case had an osteosynthesis plate during the CT scan. The screws to fixate the plate left holes in the bone model, which affects the mesh characteristics and disturbed the algorithm's proper determination of the centerline curve. Because of this, patient case 13 was excluded from further evaluation. For the remaining patient cases, the optimization ran smoothly. The runtime of the algorithm with the settings $n_{population} = 24$ and $n_{iterations} = 16$ varied between 74 minutes and 81 minutes.

The decrease in the bone protrusion score (BP score) throughout the optimization is illustrated in the plots in Appendix B. It should be noted that the BP score is the sum of the proximal and distal BP near the osteotomy plane. Final BP scores after optimization ranged between 1.547 mm (Pt 12) and 6.823 mm (Pt 4). In Figure 6.1, these patient cases with minimal and maximal BP scores are visualized. This score indicates the average residual alignment error in the range around the osteotomy plane. A larger BP score implies that the proximal and distal bone pathological bone parts are less accurately aligned and protrude more from the reference bone.

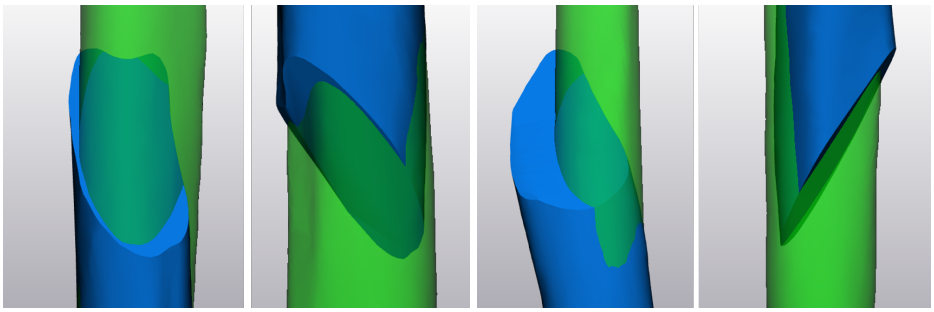

(a) Patient case 12, minimal bone protrusion. *Left: proximal part, right: distal part.*

(b) Patient case 4, maximal bone protrusion. *Left: proximal part, right: distal part.*

Figure 6.1: Example of patient cases with minimal and maximal BP scores after optimization. *Green: reference bone, blue: pathological bone after reduction.*

From the plots in Appendix B it can be observed that the total decrease in BP score varies across cases, ranging from 0.12 mm in case 12 to 2.83 mm in case 3. Moreover, the number of times the BP score decreases differs among cases, varying from 4 to 10 times throughout the optimization.

For each patient case, the planning$_{automatic}$ consisted of three plans based on the three distal alignment percentages 15, 25, and 100. This yielded a total of 42 osteotomy plans. In some of the plannings$_{automatic}$, the proximal and distal part of the bone after the osteotomy cut did not have contact at all. In these cases, the distal part of the bone protruded to an extent that the contour of the bone was completely interrupted. An example of this is visualized in Figure 6.2. These cases (16 out of 42) were excluded before validation, because they are unfeasible. In Table A.2, these cases are shown. The lack of bone contact was observed for alignment percentages of 15 and 25, but never for an alignment percentage of 100 (meaning the entire distal part after the osteotomy cut). After this exclusion, a total of 26 osteotomy plans remained as potentially feasible. For each patient case, at least one osteotomy plan remained feasible for scoring. The osteotomy plannings from planning$_{automatic}$ are presented in Appendix A.

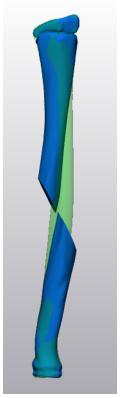

Figure 6.2: Completely interrupted bone contour. *Transparent green: reference bone, blue: pathological bone.*

6.1. Residual alignment errors

In Table 6.3, all residual alignment errors are shown for the entire bone and for the distal joint surface specifically. It should be noted that the error can be negative and positive. The error becomes negative when the pathological bone is partly "within" the reference bone. Errors are negative when they are "outside" of the reference bone model. The RMSE is calculated as the root of the squared point-wise distances between the bone models. It is therefore not influenced by negative values. The maximum and minimum errors are also given for the osteotomy plannings. These maximum values indicate the maximum error between the pathological corrected bone and the reference bone in mm's. In Table 6.1, the mean of the error calculations for the different planning methods are given. For the plannings$_{automatic}$, the mean is given for the different distal alignment percentages separately. The mean is calculated twice for the plannings$_{automatic}$: once without the plannings that were scored as unfeasible in Section 6.2 and once including all plannings.

6.1.1. Residual alignment error

From Table 6.1, it can be seen that the mean RMSE for the plannings$_{manual}$ and the plannings$_{automatic}$ with a distal alignment of 100% are very similar, with a difference of 0.002 mm. The mean RMSE for the plannings$_{automatic}$ with distal alignments of 25 and 15% are somewhat larger than that of 100% distal alignment, but not substantially. Moreover, if the unfeasible plannings are not considered when calculating the mean, the plannings$_{automatic}$ even have a lower RMSE than the plannings$_{Materialise}$. However, this calculation should be interpreted carefully, as it introduces a strong form of bias. From Table 6.3 it can be seen that for patient cases 2, 4, 5, 6, 10, and 12, the RMSE of the entire bone is smaller for the best scenario of planning$_{automatic}$ than the planning$_{manual}$. For the remaining cases, the planning$_{manual}$ has a lower residual average alignment error for the entire bone. The maximum difference in RMSE between the planning$_{manual}$ and the best scenario of planning$_{automatic}$ is 0.33 mm for patient case 6. The maximum error is lower for the best scenario of planning$_{automatic}$ for patient cases 2, 3, 4, 5, 10, and 15. For the other patient cases, the planning$_{manual}$ has a lower maximum error.

6.1.2. Distal residual alignment error

From Table 6.1, it can be seen that the mean RMSE for the distal 10% of the radius is always lower for the plannings$_{automatic}$ than for the plannings$_{manual}$, even including the cases that were scored as unfeasible. The mean maximum error for the distal 10% is also lower for the plannings$_{automatic}$. This is in accordance with Table 6.3, where it can be seen that for most patient cases the RMSE for the distal joint surface is smaller for the best scenario of planning$_{automatic}$ than the planning$_{manual}$. It can be noted for the plannings$_{automatic}$ that the smaller the distal alignment percentage, the smaller the residual RMSE. This is because the smaller the distal alignment percentage, the more focus is on aligning the distal radial joint surface. The RMSE for the distal joint surface was always below 0.8 mm, for all plannings. This implies that the alignment of the distal joint surface is very accurate.

Table 6.1: Mean of error calculations

	Mean RMSE	Mean max error	Mean RMSE distal 10%	Mean max error
Materialise	1,172	4,956	0,526	1,952
Optimization 100%	1,174	5,580	0,516	1,951
Optimization 100% feasible only	1,073	3,855	0,406	1,445
Optimization 25%	1,227	5,375	0,439	1,676
Optimization 25% feasible only	1,078	4,727	0,361	1,415
Optimization 15%	1,199	4,201	0,451	1,504
Optimization 15% feasible only	1,199	4,201	0,451	1,504

6.2. Qualitative scores

In Table 6.4, the qualitative scores are displayed. The mean score for the plannings$_{manual}$ was 7.43, whereas the score for the plannings$_{automatic}$ was 6,86 when combining all feasible plannings for the different alignment percentages. When looking at the different alignment percentages separately, the mean scores for the feasible plans were 7, 6.71, and 6.75 for the distal alignment of 100, 25, and 15% respectively. For case 3, 8, and 11, the planning$_{automatic}$ was not able to generate a feasible planning, mainly due to insufficient bone contact. Patient case 10 with an alignment % of 25 was also scored as unfeasible because of the poor bone overlap and the lack of radial bow. The remaining 22 osteotomy plans were all scored as feasible (a score of ≥6). Patient cases 1, 4, 6, and 12 scored equal for the planning$_{automatic}$ and planning$_{manual}$. For the other patient cases, the planning$_{automatic}$ consistently had a lower score compared to the planning$_{manual}$. The only exception is patient case 5, where the planning$_{automatic}$ with an alignment of 100% scored 2 points higher than the planning$_{manual}$ (8 vs. 6). The maximum difference between the planning$_{manual}$ and the best scenario of planning$_{automatic}$ was always 1 point. For the planning$_{automatic}$, the maximum score was an 8/10, compared to a 9/10 for the planning$_{manual}$. An example of a good and an unfeasible osteotomy plan are visualized in Figure 6.3. The most common reasons for low scores (6/10) were discontinuation of the bone contour, little bone overlap, complex plate position, and a sub optimal radial bow. However, it can be noted that none of the cases lacked in alignment of the distal and proximal joint surfaces, which is in accordance with the results discussed in Section 6.1.
When looking at the plannings$_{automatic}$ and the plannings$_{manual}$, the location of the osteotomy plane is very similar for all patient cases, except for patient case 14. It is remarkable that the plane from the planning$_{automatic}$ is positioned much more distal as compared to the plane in the planning$_{manual}$.

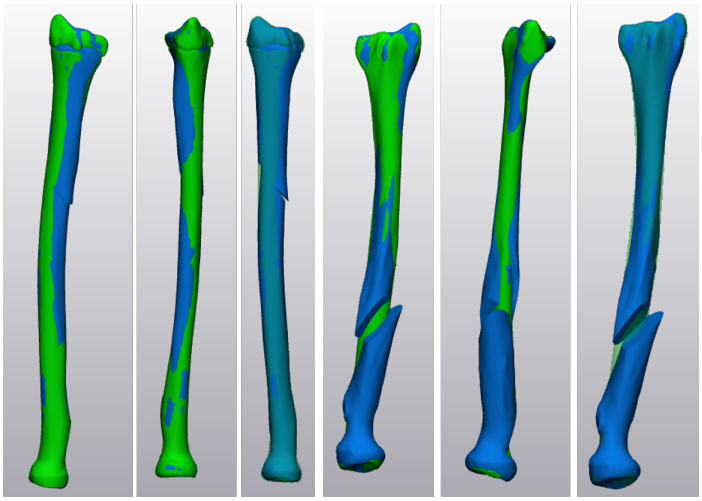

(a) Patient case 15 (b) Patient case 8

Figure 6.3: Patient case 15, alignment 100% with a qualitative score of 8/10. Patient case 8, alignment 100%, scored as unfeasible. *Blue = pathological bone, green = reference bone.*

6.3. Concordance between validation scores

In Table 6.2, a comparison is made between the validation scores for each patient case. It can be seen that the residual average alignment error and the qualitative score do not always indicate the same planning method to be best. For example, for patient case 2 and 10 the RMSE for the entire bone is lower for the planning$_{automatic}$ while the qualitative score favors the planning$_{manual}$. Also important to note is the correlation between the RMSE score for the entire bone and the qualitative score. In Figure 6.4, the qualitative scores are plotted against the RMSE scores. From this plot, it can be seen that a low correlation is found.

6.4. Repeatability

The optimization was run twice for patient case 3. This patient case was chosen because it was scored as unfeasible, so it is interesting to see whether a new run might improve the results. In Figure 6.5, it can be seen that the generated osteotomy plans are quite different for the two runs. From run 2, an open wedge osteotomy resulted, whereas run 1 did not yield an open wegde. In both cases, the bone overlap is very poor. Figure 6.6 shows the decrease in BP score throughout the optimization for the two runs. It is clear that the course of the BP score is different for both runs and the final BP score is 0.3 mm lower for the first run. Also, for the second run the BP score decreased 14 times instead of 6 times in run 1.

Table 6.2: Comparison of best score between planning$_{manual}$ and the best scenario of planning$_{automatic}$ per patient case

	Residual average alignment error	**Qualitative score**
Pt1	planning$_{manual}$	Equal
Pt2	planning$_{automatic}$	planning$_{manual}$
Pt3	Equal	planning$_{manual}$
Pt4	Equal	Equal
Pt5	planning$_{automatic}$	planning$_{automatic}$
Pt6	planning$_{manual}$	Equal
Pt7	planning$_{manual}$	planning$_{manual}$
Pt8	planning$_{manual}$	planning$_{manual}$
Pt9	planning$_{manual}$	planning$_{manual}$
Pt10	planning$_{automatic}$	planning$_{manual}$
Pt11	planning$_{manual}$	planning$_{manual}$
Pt12	Equal	Equal
Pt14	Equal	planning$_{manual}$
Pt15	planning$_{manual}$	planning$_{manual}$

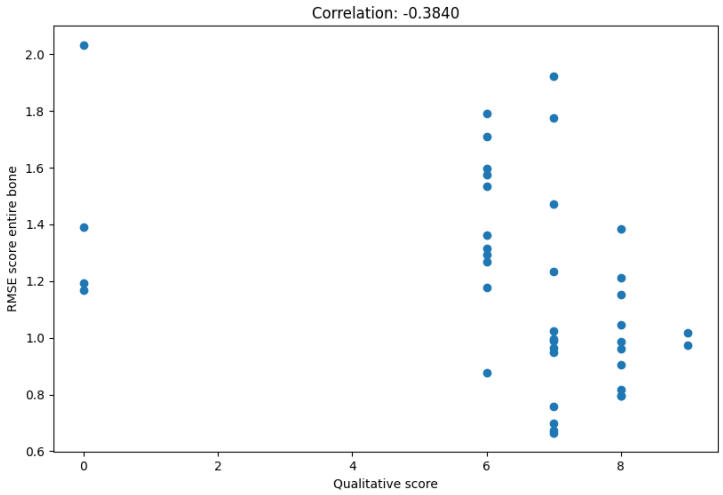

Figure 6.4: Correlation between the qualitative scores and the RMSE scores for all osteotomy plannings. Qualitative score 0 means unfeasible.

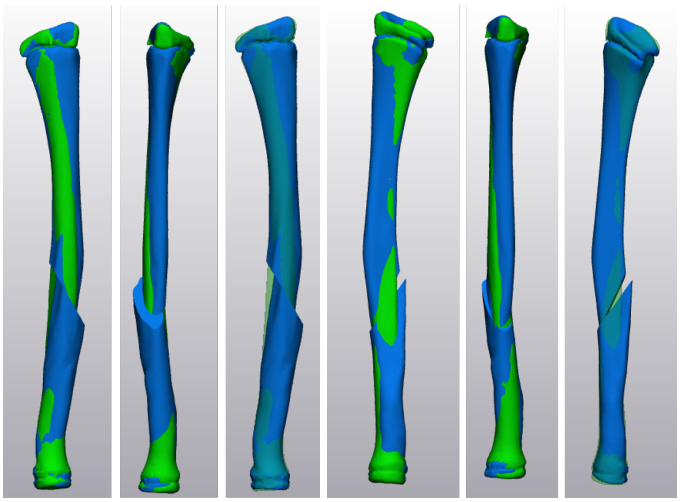

(a) Run 1 (b) Run 2

Figure 6.5: Patient case 3, osteotomy plan for two different runs. *Blue = pathological bone, green = reference bone.*

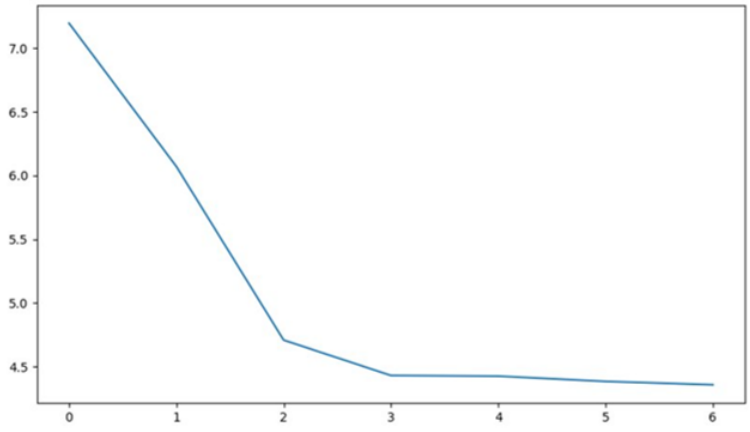

(a) Run 1

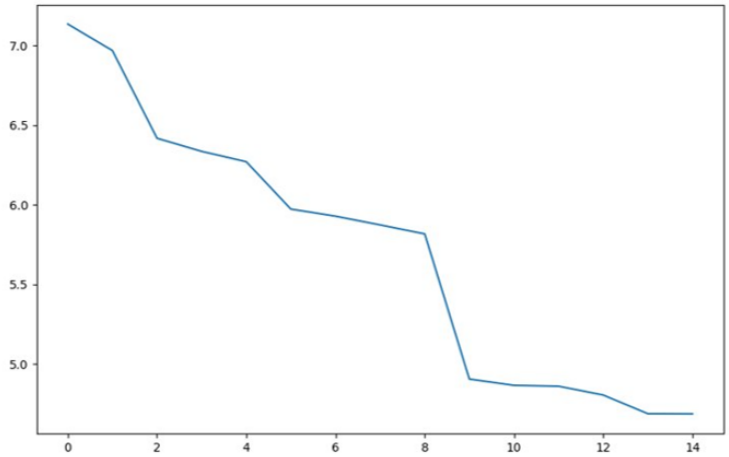

(b) Run 2

Figure 6.6: Patient case 3, decrease in BP score for two different runs.

Table 6.3: Residual average alignment errors (RMSE) for each patient case with min and max values

Patient case	Alignment %	RMSE	min	max	$RMSE_{distal\ 10\%}$	min	max
Pt 01 Materialise		0,7963	-1,5433	3,2375	0,4632	-1,0891	1,6413
Pt 01 optimization	100	0,8179	-2,4346	4,1759	0,4265	-1,3876	1,5711
Pt 02 Materialise		1,924	-3,3184	6,3252	0,5903	-1,2946	1,8798
Pt 02 optimization	100	1,7912	-3,561	5,8962	0,5459	-1,095	1,7642
Pt 02 optimization	25	1,7098	-3,8509	5,8763	0,4855	-0,9174	1,2456
Pt 03 Materialise		1,3853	-3,1146	5,307	0,7595	-3,1146	2,1109
Pt 03 optimization	100	1,3911	-4,7314	5,0645	0,7189	-3,1802	1,9758
Pt 04 Materialise		1,3156	-3,1175	5,9567	0,7793	-2,4866	1,5473
Pt 04 optimization	100	1,2945	-4,1649	5,9452	0,7922	-2,303	1,9348
Pt 05 Materialise		0,8762	-1,3815	3,2846	0,3894	-1,1362	1,7569
Pt 05 optimization	100	0,7944	-1,4629	3,2621	0,4177	-1,4629	1,3914
Pt 05 optimization	25	1,1781	-3,6013	4,751	0,3126	-1,0335	1,37
Pt 06 Materialise		1,598	-2,8381	6,8688	0,3661	-1,2256	1,0383
Pt 06 optimization	100	1,2683	-2,3616	6,9654	0,4052	-1,5683	1,1431
Pt 07 Materialise		0,9042	-2,179	4,9753	0,3862	-1,1017	1,3547
Pt 07 optimization	100	0,9642	-4,2527	5,4755	0,3377	-1,0305	1,1021
Pt 07 optimization	25	1,3616	-5,2705	7,8549	0,3085	-1,0347	0,9433
Pt 07 optimization	15	1,5345	-5,0185	8,232	0,2843	-1,2052	0,9069
Pt 08 Materialise		1,7748	-2,3005	5,2773	0,3576	-1,7664	0,9965
Pt 08 optimization	100	2,0336	-5,1208	9,3719	0,3634	-1,7385	0,9147
Pt 09 Materialise		1,2106	-1,8484	5,2514	0,418	-1,3023	0,9016
Pt 09 optimization	100	1,2347	-1,6539	5,5712	0,4477	-1,6323	1,1453
Pt 09 optimization	25	1,4709	-4,366	6,392	0,2591	-0,8034	0,6965
Pt 10 Materialise		0,9613	-2,9838	6,3232	0,7272	-1,5854	2,7098
Pt 10 optimization	100	0,9492	-4,2872	6,0596	0,6752	-1,9691	2,1955
Pt 10 optimization	25	1,1924	-5,1783	5,1273	0,6197	-1,4133	2,0885
Pt 11 Materialise		0,9974	-3,6874	4,8193	0,5563	-2,19	0,9832
Pt 11 optimization	100	1,1669	-4,4754	7,9035	0,5553	-2,2634	0,9394
Pt 12 Materialise		0,672	-2,8122	2,2583	0,4217	-1,5723	1,666
Pt 12 optimization	100	0,6653	-2,6393	2,5029	0,4257	-1,8212	1,8948
Pt 12 optimization	25	0,7587	-2,5914	2,5029	0,4193	-1,8027	1,8768
Pt 12 optimization	15	0,6979	-2,5914	2,5029	0,4281	-1,7516	1,8569
Pt 14 Materialise		0,9754	-2,5106	3,7683	0,5646	-1,5586	1,7041
Pt 14 optimization	100	1,0235	-3,1579	4,8259	0,5462	-1,6587	2,2065
Pt 14 optimization	25	0,9892	-3,1579	4,8259	0,5577	-1,7361	2,3015
Pt 14 optimization	15	0,9873	-3,1579	4,8259	0,5435	-1,6855	2,2225
Pt 15 Materialise		1,0193	-3,3071	5,1647	0,5789	-2,1491	2,5276
Pt 15 optimization	100	1,0457	-2,4299	4,9696	0,5603	-2,0228	2,4279
Pt 15 optimization	25	1,1527	-2,2163	5,5282	0,5464	-1,8761	2,6864
Pt 15 optimization	15	1,5743	-4,6745	6,3377	0,5498	-1,5372	3,1413

Table 6.4: Scores for each patient case by dr. J. W. Colaris

Patient	Planning	Alignment %	Score	Explanation
1	planning$_{manual}$		8	Overall good
1	planning$_{automatic}$	100	8	Good bone overlap Some protrusion Increased radial bow
2	planning$_{manual}$		7	Increased radial bow Sufficient overlap Feasible approach
2	planning$_{automatic}$	100	6	Increased radial bow Discontinuous bone contour, can be cut off Sufficient overlap Feasible approach
2	planning$_{automatic}$	25	6	Increased radial bow Discontinuous bone contour Reasonable bone overlap Just about feasible
3	planning$_{manual}$		8	Overall good
3	planning$_{automatic}$	100	Unfeasible	Insufficient bone overlap Overcorrection
4	planning$_{manual}$		6	Discontinuous bone contour, can be cut off Suboptimal position for plate fixation Just about feasible
4	planning$_{automatic}$	100	6	Increased radial bow Discontinuous bone contour, can be cut off Sufficient bone overlap Just about feasible
5	planning$_{manual}$		6	Osteotomy is very good Very complex plate position , too proximal Requires Thompson approach vs. Henry approach
5	planning$_{automatic}$	100	8	Sufficient bone overlap Suboptimal plate position Good radial bow Little discontinuation of bone contour
5	planning$_{automatic}$	25	6	Just about feasible
6	planning$_{manual}$		6	Discontinuous bone contour, can be cut off Complex plate position Technically feasible
6	planning$_{automatic}$	100	6	Increased radial bow Sufficient bone overlap Discontinuous bone contour, can be cut off
7	planning$_{manual}$		8	Overall good
7	planning$_{automatic}$	100	7	Proximal and distal alignment good Sufficient bone overlap Approach is feasible Slightly decreased radial bow
7	planning$_{automatic}$	25	6	Just about feasible
7	planning$_{automatic}$	15	6	Little bone contact Discontinuous bone contour Just about feasible
8	planning$_{manual}$		7	Sufficient bone overlap Discontinuous bone contour Feasible
8	planning$_{automatic}$	100	Unfeasible	Not sufficient bone overlap Open wedge with too little bone contact
9	planning$_{manual}$		8	Overall good
9	planning$_{automatic}$	100	7	Sufficient bone overlap Good radial bow
9	planning$_{automatic}$	25	7	Discontinuous bone contour, can be cut off Good radial bow Sufficient bone overlap
10	planning$_{manual}$		8	Overall good
10	planning$_{automatic}$	100	7	Just about sufficient bone overlap Good radial bow
10	planning$_{automatic}$	25	Unfeasible	Lack of radial bow Bone overlap is poor
11	planning$_{manual}$		7	Discontinuous bone contour, can be cut off Obliqueness is feasible
11	planning$_{automatic}$	100	Unfeasible	Too much discontinuation of bone contour Insufficient bone overlap
12	planning$_{manual}$		7	Increased radial bow Sufficient bone overlap Feasible
12	planning$_{automatic}$	100	7	Bone overlap is sufficient Approach is feasible Plate position is feasible
12	planning$_{automatic}$	25	7	Moderate radial bow Sufficient bone overlap
12	planning$_{automatic}$	15	7	Sufficient bone overlap Good radial bow Complex for plate fixation, but feasible
14	planning$_{manual}$		9	Very good
14	planning$_{automatic}$	100	7	Lacking in radial bow
14	planning$_{automatic}$	25	7	Lacking in radial bow
14	planning$_{automatic}$	15	8	Radial bow is restored Sufficient bone overlap
15	planning$_{manual}$		9	Very good
15	planning$_{automatic}$	100	8	Overall good
15	planning$_{automatic}$	25	8	Overall good Little discontinuation of bone contour
15	planning$_{automatic}$	15	6	Decreased radial bow Sufficient bone overlap Discontinuous bone contour

7
Discussion

The multidimensional complexity of correcting forearm malunions has led to an increased use of computer-assisted 3D preoperative planning. Despite the strong advantages that are associated with it like improved understanding of the deformity and high accuracy, the clinical application remains limited due to the required time, effort and expertise. This research aimed to answer the question

How can the computer-assisted patient-specific corrective osteotomy planning for forearm malunions be automated and optimized?

To this end, an automatic tool was developed to enhance the use of computer-assisted preoperative planning for malunions of the radius. The tool automatically registers the bone models to give the user an insightful analysis of the degree and nature of deformity. In the second part of this research, an Evolutionary Algorithm was implemented to optimize the osteotomy plane location and orientation. The automatically generated patient-specific osteotomy plannings minimize the bone protrusion near the osteotomy plane and guarantee accurate proximal and distal radial joint surface alignment. Per patient case, three final osteotomy plans are provided to the user, that balance between distal radial joint surface alignment and restoration of the radius shape. The user can choose the osteotomy plan that best satisfies the patient-specific osteotomy goals. Based on the validation performed on 15 patient cases, it can be concluded that the automatic tool is capable of yielding clinically feasible plannings. The residual average alignment errors of the entire radius shape do not deviate substantially from those of plans that have been accepted in the past. Moreover, the distal radial joint surface alignment for the osteotomy plans generated by the automatic tool is very accurate.

7.1. Strengths and limitations

The developed automatic tool offers several key advantages, primarily the required minimal user interaction. As a result, the time investment needed is significantly reduced. Within a short time, numerous osteotomy plans can be computed and evaluated, surpassing the time investment required for human trial-and-error.This computational capacity has a significant advantage over the time investment for human trial-and-error. Despite the minimal user interaction, the tool still involves the user during critical decision points by presenting different scenarios for comparison. This approach leverages the user's experience and consideration of patient-specific factors, enabling their contribution to the final osteotomy plan. Furthermore, it allows for a comparison of various osteotomy plans based on insights into different trade-offs.

An additional noteworthy feature of the developed automatic planning tool is its flexibility regarding the type of osteotomy. It allows both closing and open wedges, as well as single-cut rotational osteotomies. The type of osteotomy is determined by the minimal bone protrusion near the osteotomy plane while securing accurate distal radial joint surface alignment. This ensures osteotomy plans that are in line with the anatomic reconstruction goals.

Another significant benefit of the developed automatic tool is its ability to guarantee accurate distal radial joint alignment. Joint alignment is crucial for restoring forearm function. In the study conducted by Carrillo et al. that also focused on optimizing preoperative planning for corrective forearm osteotomies, a mean RMSE of 0.94 mm was found for the distal landmarks [14]. Comparatively, in this research, the mean RMSE for the alignment of the distal 10% of the radius was 0.516 mm with a distal alignment of 100%. This suggests that the automatic planning tool developed in this research achieves more precise results for distal radial joint surface alignment.

This research establishes a foundation for a framework to automatically optimize corrective osteotomy planning for radius malunions. It can be further developed and improved upon, allowing for adjustments or additions such as the implementation of clinical constraints or expanding the objective function.

Ultimately, the feasibility of an osteotomy plan appears to depend on various factors that were considered in this research. In the following subsections, the limitations of this research are discussed, that can provide insights into the reasons for the lack of feasibility of some of the osteotomy plans. Shortcomings of the optimization algorithm

itself and clinical feasibility aspects are reviewed, and potential solutions to address the limitations are suggested.

7.1.1. Initial population

When analyzing the optimization process, it is noteworthy that the improvement in the bone protrusion score is only marginal across generations. One possible explanation for this is that within the initial population, due to the size and genetic diversity, a solution is already relatively optimal. The initial population consists of 26 different solutions, which are generated and compared to each other. If one of these solutions is already close to optimal, further improvement in subsequent generations will be limited. On the other hand, the initial population may also negatively impact the optimization result, as it critically affects the convergence and performance of the algorithm [65]. To address this issue, the Halton sequence was utilized to generate the initial population, as described in Subsection 4.3.1. Nonetheless, the problem remains that the initial population's combinations of plane locations and orientations may affect the recombination possibilities for the following generations. Therefore, it can be concluded that the initial population plays a critical role in determining the optimization result, and that a larger population size might contribute to better results.

7.1.2. Similarity of bones

Another aspect that must be considered when using optimization to plan osteotomy for malunited forearm fractures is the similarity between the pathological bone and the contralateral bone. If the two bones differ in shape even before the malunion, the optimization result will be adversely affected by this, resulting in a poorer outcome. Similarly, if the patient currently has an osteosynthesis plate fixated, the 3D model may be distorted, leading to problems during the optimization process. Additionally, if the contralateral bone is also fractured or malunited, it cannot be used as a planning target. In these cases, the contralateral bone can not be used as a planning target. An alternative approach could involve using statistical shape models (SSMs). SSMs are geometric models that represent an average shape of many three-dimensional objects, as well as their variation in shape [66]. Studies suggest that SSMs can be used to accurately predict the patient-specific anatomy, and could thus serve as a useful planning target in cases of bilateral fractures [67].

7.1.3. Control parameters

One of the most complicated aspects of the implemented EA in this research is the settings for the control parameters. These are the parameters that control certain processes in the optimization. Many of these parameters are present like $n_{population}$, n_{elites}, $r_{crossover}$, $r_{mutation}$ and k_{sp}. All processes in the optimization algorithm and thus the overall performance are dependent on the values of these parameters. Also, the type of selection, crossover, and mutation influence the optimization. In addition, some parameters affect the performance more than others [68]. Moreover, these control parameters interact in a complex way [69]. To give an example, changes in different parameters can lead to similar effects. If the selection pressure k_{sp} is set higher, i.e. the chance of a chromosome to be selected becomes smaller, convergence will occur sooner in the process. This can lead to getting stuck in local minima. Lowering the $r_{mutation}$ can also lead to getting stuck in local minima. The settings for the control parameter values are dependent on the optimization problem specifically and the characteristics of the population. Moreover, most of the control parameters have to be balanced carefully. Often, concessions have to be made that either result in early convergence or in maintaining diversity in the population. Computational time and population diversity also stress the trade-off that has to be made when determining the values for the control parameters. It is hard to determine the optimal values for these parameters. A thorough understanding of all control parameters and their effects and interactions is required. Tuning the values is possible through trial-and-error. This would require extensive analysis of the effects of changing each parameter. One method to alleviate a part of this problem, is by estimating the entropy of the parameters. Entropy could be used as an indicator for the relevance of the different parameters [68]. From this, certain parameters can be given more time/capacity in tuning than others.
It can be concluded from this that one of the main limitations in this study is the likeliness that the values of the control parameters are sub optimal. As long as these parameters are not tuned accurately, the result of the optimization will not be optimal.

7.1.4. Population size and number of iterations

Two control parameters that are likely to be insufficient in this research are the population size $n_{population}$ and the number of iterations $n_{iterations}$. The population size and the number of iterations in this study are set rather small to reduce computational time. One run with $n_{population}$ = 24 and $n_{iterations}$ = 16 already can take up to 80 minutes. An experiment with 24 iterations doubled the runtime, from which it can be concluded that expanding the number of iterations exponentially increases the runtime. It is known that a larger population size can maintain the diversity in the population. Diversity promotes exploration of the solution space because it delays convergence. [70]. This results in accuracy of getting an optimal solution [71]. Secondly, diversity also helps to locate multiple optima in the case that more than one optimal solution is present [70]. This applies for corrective osteotomies especially, because not just one solution is feasible. A larger number of iterations gives the algorithm more opportunities to improve and thus reach a better solution. This probably does not apply until infinity: at one point the optimum will be reached

and no other solution will result in improvement. However, it should be noted that increasing these parameters excessively can result in unfeasible runtimes, which would contradict the purpose of the research. Therefore, a balance must be found between computational efficiency and the accuracy of the solution.

7.1.5. Objective function

Another important limitations in this research is the defined objective function. Fitness landscapes in optimization are defined by the objective function, meaning that an inadequate objective function can result in a search problem that lacks feedback suggesting where to look for a solution [72]. In this research, the objective function is defined by the calculation of the bone protrusion near the osteotomy plane. This objective function is limited in several ways. First of all, the bone protrusion is calculated as a function of the osteotomy plane. This osteotomy plane is dependent on 4 variables, namely the plane location along the z-axis, and the plane orientation in the x-, y-, and z-direction. The bone protrusion scores determine the likelihood that a chromosome passes on to the next generation. However, the problem here is that a solution with a sub optimal plane location can be compensated for with a good plane orientation, or the other way around. Because of this, solutions with sub optimal values for certain variables might be assumed as good, due to their fitness score. These variable values are then passed on to the next generations, resulting in suboptimal solutions. The algorithm might even get stuck in local minima because of this.

Another limitation is that the bone protrusion is only calculated near the osteotomy plane. If the residual deformity, like a decreased radial bow, is located further away from the osteotomy plane, the bone protrusion score might be good while the radius shape is still not properly restored. An alternative would be calculating the bone protrusion for the entire length of the bone. This is also not ideal, as the the RMSE is an average of all point-wise errors. This means that if the error is small along a large part of the bone but the bone protrudes extremely near the osteotomy plane, the RMSE might be relatively low. Moreover, from the low correlation between the RMSE score for the entire bone and the feasibility score, it appears that using the RMSE for the entire bone is not perfectly suitable either. An example can be seen for patient case 11. The RMSE for the entire bone is 1.167 mm, which is not extremely high. However, the planning has been scored as unfeasible, due to extensive discontinuation of the bone contour and insufficient bone overlap. The bone protrusion score does capture this, because it focuses on the area near the osteotomy plane. This comparison indicates the balance that has to be found when drawing up the objective function.

A final limitation of the defined objective function, it that it is a rather simplified version of the actual corrective osteotomy goal. In this optimization algorithm, a proper distal radius joint surface alignment is guaranteed, and the algorithm will search for a solution with minimal bone protrusion. To this end, it is assumed that restoration of the anatomy will result in proper forearm function. However, the goals of the osteotomy are not just limited to the alignment of the joints and the restoration of the shape. From the qualitative scores reported in Section 6.2, it appears that contact between the two bone parts after the osteotomy cut is an important objective that is often lacking in the results of this optimization. This is complicated to implement, as it would easily constrain the type of osteotomy. For instance, if excessive bone shortening has occurred as a result of the malunion, these gaps might be necessary to reach proper bone alignment. Adding a hard constraint to the distance between the two bones would reduce the generalizability of the optimization. For one case, some space between the two parts would be clinically feasible or even preferable, whereas for other cases this should be avoided. Implementing constraints like these should be patient-specific and thus set by the user.
From the qualitative scores it can also be seen that the algorithm often results in discontinuation of the bone contour. This can cause problems with the soft tissues surrounding the radius. Generally speaking, this can be fixed by sawing the protruding part off. However, if it becomes too extensive, the osteotomy plan might be unfeasible. Implementing certain constraints for this could contribute to a more clinically realistic objective function.
Another addition to the objective function would be also considering the osteosynthesis plate fixation. For fixing the plate and screws, the surface has to be somewhat smooth between the proximal and distal bone part. One way to implement this is by requiring continuity of the surfaces. Another method would be to require continuity of the centerline curve of the proximal and distal part near the osteotomy plane. However, the latter would not necessarily mean that the bone surfaces are continuous, as the pathological bone can be thicker than the reference bone. Also, the position of the plate must considered. If the plate has to be fixated on the volar side too close to the proximal joint, it might give problems with flexing the elbow.

7.1.6. Repeatability

An important shortcoming of EAs is that they can not guarantee convergence to the global optimum. However, for this research specifically, multiple optima will be present. Different combinations of osteotomy plane locations and orientations could yield very similar scores and might be clinically equally feasible. It is hard to draw conclusions about the repeatability, because it was not properly analyzed in this research. To test the repeatability, one patient case was run twice, which resulted in a slightly different bone protrusion score and a different osteotomy plan. This insinuates that the optimization algorithm is not yet highly repeatable. However, clinical relevance should also be considered. One tenth of a mm difference in scores does not necessarily mean superiority from a clinical perspective. Cases like

this will need a user to judge based on patient-specific factors. The advantage of this is that the repeatability does not have to be perfect. If the optimization does not result in the exact same osteotomy plan each time it is run, it could still perform well. However, if significant differences in solutions occur, this can be a problem. Repeatability is important in the sense that each time the optimization is run, an optimal result should be found. The stochastic nature of EAs already contributes to this; through mutation the algorithm is able to avoid getting stuck in local minima [65]. The concept of "going multi optimal" could also be interesting. In that case, multiple optimal results are obtained, so that the user can be provided with a variety of different options [72]. This concept could be realized by making use of *niching methods*. These methods aim at obtaining parallel convergence towards different optimal solutions, by maintaining the diversity within a population [72]. An example of such a niching technique is fitness sharing. In this technique, chromosomes that have similar members within the population are penalized via their fitness [72]. Preference is given to solutions in sparsely populated regions of the search landscape if the solutions are of similar fitness to those in densely populated regions. The aim of this is to keep diversity in the population.

7.1.7. Generalizability

Determining the generalizability of the optimization algorithm is complex. The generalizability of an algorithm is the ability to be insensitive to changing certain parameters [73]. For this research, it can be interpreted as the ability to yield stable results (osteotomy plans) if new data is given that might deviate from the data the algorithm was developed on. The optimization algorithm works on all patient cases, except for one. From this, it can be concluded that the generalizability is not yet optimal. Patients with forearm malunions are likely to have osteotsynthesis plates and thus screws in their radius, so this should not influence the optimization. However, preprocessing steps like wrapping the holes could be relevant. Nonetheless, further improving the generalizability is a relevant implementation that must be made to enhance the clinical usefulness of the automatic tool.

7.1.8. Clinical considerations

Besides limitations in the optimization algorithm itself, some clinical considerations must be taken into account for this research. The main limitation of the implemented optimization is that it does not consider the relationship between the radius and the ulna. When planning a corrective osteotomy of the forearm, the relation to the neighboring bone should always be considered. If radial shortening has occurred, the radial inclination might be compromised. In that case, the malunited radius should be planned towards the contralateral radius. However, if the ulna of the pathological forearm is also shorter and the length difference between the malunited radius and the ulna is negligible, the contralateral radius should be scaled. Otherwise, the malunited radius would be planned towards the longer contralateral radius. This would eventually result in a radius that is too long for the ulna. This will give problems in the DRUJ, as the radius and ulna can not articulate properly.

The implemented optimization also lacks the involvement of soft tissue. Studies have demonstrated that the function may still be limited despite anatomic fracture reduction due to soft tissue contracture [9]. For example, central band contracture can affect the function of the forearm [48].

Also important to consider is the type of osteotomy. In the automatic tool developed in this research, the type of osteotomy is not restricted. In some of the patient cases, a closing wedge osteotomy resulted as the optimal plan. To realize this, a second cut is required to remove the wedge. This is not yet implemented in the automatic tool, but should be for completeness. Moreover, the implemented optimization is restricted to a single-cut osteotomy. In some complex malunion cases, a double cut is required to fully restore the anatomy. Despite the fact that a single-cut osteotomy is preferred over a double-cut, a double-cut osteotomy should also be included in the algorithm for completeness. However, this will require many extra variables and will result in much higher computational time and a more complex objective function.

An essential note regarding the location of the osteotomy plane should be made. In the automatic tool, the user is asked to indicate the center of the malunion. Based on this, the boundaries for the osteotomy plane are determined as 10% proximal and distal of the center of the malunion. As discussed before, the osteotomy cut is often made near the center of the malunion because this is the location of maximal deformity. However, the osteotomy plan that is generated by the automatic tool is thus dependent on the location that the user appoints as the center of the malunion. For patient case 14, it can be seen that the location of the osteotomy plane differs between the two plannings methods. This can likely be attributed to a mistake in the indication of the center of the malunion.

Finally, when interpreting the results of this research, it should be taken into account that the number of patient cases that were used for validation is rather small. To properly test the accuracy, more patient cases should be considered. This would also contribute to the generalizability of the automatic tool. Before eventually using the automatic tool, a clinical study must be conducted to prove clinical relevance.

7.2. Clinical Relevance

This project's clinical relevance lies primarily in the significant reduction of time required for osteotomy planning. The automatic optimization algorithm developed in this research minimizes user interaction, saving a considerable amount of time that would otherwise be spent performing iterative trial-and-error tasks. This aspect can enhance the clinical application of preoperative computer-assisted osteotomy planning, which is currently limited. However, the clinical relevance will only become significant once the optimization is based on an objective function that is comprehensive from both a technical and clinical point-of-view. The optimization is currently bounded by the shortcomings that have been discussed in the previous section. If these limitations can be overcome, accurate anatomical restoration can be guaranteed. A next step could be the integration with the kinematic models delivered by Derek van Loon [48]. This would allow the evaluation of the outcomes of an osteotomy plan in a kinematic model. This can highly contribute to the clinical relevance of this research, resulting in osteotomy plans that can be evaluated preoperatively on both anatomical and functional feasibility aspects. Moreover, the automatic workflow can be further expanded to the design of surgical guides. Surgical guides can enhance the clinical application by the accurate translation of the preoperative plan to the surgery.

Although the developed automatic optimization workflow may currently lack accuracy and generalizability, it provides an excellent starting point for future research. The algorithm can provide an initial estimation of an osteotomy plan, which can be further improved manually. Additional features can be added to enhance the algorithm's performance, building on the framework presented in this research. Overall, this research provides a foundation for improving the efficiency and efficacy of osteotomy planning, benefiting both clinicians and patients.

8

Conclusions and Future Recommendations

In this research, a tool for the automation and optimization of patient-specific corrective osteotomy planning for radius malunions was developed. The automatic tool determines the nature and degree of deformity automatically through the registration of the pathological and reference bone. Based on this, the optimal osteotomy plan can be generated. To this end, an Evolutionary Algorithm was implemented that generates, explores, and evaluates various osteotomy plans. The algorithm progresses based by minimizing the bone protrusion while ensuring alignment of the proximal and distal radial joint surfaces. The optimization yields a patient-specific osteotomy plan, including the plane location, orientation, and the required reduction of the distal part after the osteotomy cut. Three osteotomy plans are provided to the user, who can select the one that best satisfies the patient-specific osteotomy goals.

The validation of the automatic tool was conducted using fifteen patient cases of forearm malunions that were previously planned. The runtime was about 75 minutes per patient case. Fourteen out of fifteen cases resulted in error-free osteotomy plans. The residual alignment errors were calculated to objectively compare the outcomes of the different plannings methods. Differences were small, but usually in favour of the manually planned osteotomies. The automatic tool consistently generated osteotomy plans with residual average distal radial joint surface alignment errors below 0.8 mm. To incorporate clinical experience and knowledge regarding the feasibility of the osteotomy plans, qualitative scores were assigned by Dr. Colaris, who was blinded to the type of planning. Among the fourteen patient cases, three were deemed unfeasible. For the remaining eleven cases, the best scenario of the optimized osteotomy plans scored similar or 1 point lower than the manual plannings. The most common aspects that the optimized osteotomy plans lacked were poor bone overlap and a discontinuous bone contour.

From the validation results, it can be concluded that the developed automatic tool is capable of generating clinically feasible osteotomy plans, although it is not yet accurate and generalizable enough for clinical use. The framework requires expanding the objective function and tuning the control parameters to improve the results. Additionally, further enhancements are needed in terms of clinical feasibility, such as considering the plate position, bone contact, and continuous bone contour.

In summary, the framework developed in this research provides a good foundation for the automated optimization of computer-assisted planning of corrective osteotomies for malunions, while respecting the individual's anatomy. While the automatic tool developed in this research might not yet be ready for clinical practice, it can provide initial osteotomy plans that can be further adjusted according to the user's experience and knowledge. The proposed workflow has the potential to significantly enhance the efficiency of corrective osteotomy planning, paving the way for more effective treatment of forearm malunions.

Reference list

[1] *Polygon mesh,* https://en.wikipedia.org/wiki/Polygon_mesh (2023), accessed: 2023-04-25.

[2] N. Assink, A. M. L. Meesters, K. ten Duis, J. S. Harbers, F. F. A. IJpma, H. C. van der Veen, J. N. Doornberg, P. A. J. Pijpker, and J. Kraeima, *A two-step approach for 3d-guided patient-specific corrective limb osteotomies,* Journal of Personalized Medicine **12** (2022), 10.3390/jpm12091458.

[3] M. J. Richard, D. S. Ruch, and J. M. Aldridge, *Malunions and nonunions of the forearm,* Hand Clinics **23**, 235 (2007), forearm Injuries.

[4] B. Saravi, G. Lang, R. Steger, A. Vollmer, and J. Zwingmann, *Corrective osteotomy of upper extremity malunions using three-dimensional planning and patient-specific surgical guides: Recent advances and perspectives,* Frontiers in Surgery **8** (2021), 10.3389/fsurg.2021.615026.

[5] J.-M. Cognet and O. Mares, *Distal radius malunion in adults,* Orthopaedics Traumatology: Surgery Research **107**, 102755 (2021), 2020 Instructional Course Lectures (SoFCOT).

[6] B. Bushnell and D. Bynum, *Malunion of the distal radius,* The Journal of the American Academy of Orthopaedic Surgeons **15**, 27 (2007).

[7] L. Nagy, L. Jankauskas, and C. E. Dumont, *Correction of forearm malunion guided by the preoperative complaint,* Clinical Orthopaedics and Related Research **466** (2008), 10.1007/s11999-008-0234-3.

[8] B. Saravi, G. Lang, R. Steger, A. Vollmer, and J. Zwingmann, *Corrective osteotomy of upper extremity malunions using three-dimensional planning and patient-specific surgical guides: Recent advances and perspectives,* Frontiers in Surgery **8** (2021), 10.3389/fsurg.2021.615026.

[9] P. Jayakumar and J. Jupiter, *Reconstruction of malunited diaphyseal fractures of the forearm,* HAND **9**, 265–273 (2014).

[10] A. M. Byrne, B. Impelmans, V. Bertrand, A. V. Haver, and F. Verstreken, *Corrective osteotomy for malunited diaphyseal forearm fractures using preoperative 3-dimensional planning and patient-specific surgical guides and implants,* Journal of Hand Surgery **42** (2017), 10.1016/j.jhsa.2017.06.003.

[11] S. Kemp, *Osteotomy and grafting of the distal radius using virtual planning and patient specific guides,* BMC Proceedings **9** (2015), 10.1186/1753-6561-9-s3-a96.

[12] G. A. Buijze, N. Leong, F. Stockmans, P. Axelsson, R. Moreno, A. Sörensen, and J. Jupiter, *Three-dimensional compared with two-dimensional preoperative planning of corrective osteotomy for extra-articular distal radial malunion: A multicenter randomized controlled trial,* The Journal of bone and joint surgery. American volume **100**, 1191 (2018).

[13] K. Roth, E. van Es, G. Kraan, D. Eygendaal, J. Colaris, and F. Stockmans, *Accuracy of 3d corrective osteotomy for pediatric malunited both-bone forearm fractures,* Children **10** (2023), 10.3390/children10010021.

[14] F. Carrillo, S. Roner, M. von Atzigen, A. Schweizer, L. Nagy, L. Vlachopoulos, J. G. Snedeker, and P. Fürnstahl, *An automatic genetic algorithm framework for the optimization of three-dimensional surgical plans of forearm corrective osteotomies,* Medical Image Analysis **60** (2020), 10.1016/j.media.2019.101598.

[15] N. L. Leong, G. A. Buijze, E. C. Fu, F. Stockmans, and J. B. Jupiter, *Computer-assisted versus non-computer-assisted preoperative planning of corrective osteotomy for extra-articular distal radius malunions: A randomized controlled trial,* BMC Musculoskeletal Disorders **11** (2010), 10.1186/1471-2474-11-282.

[16] G. Caiti, J. G. Dobbe, S. D. Strackee, G. J. Strijkers, and G. J. Streekstra, *Computer-assisted techniques in corrective distal radius osteotomy procedures,* IEEE Reviews in Biomedical Engineering **13** (2020), 10.1109/RBME.2019.2928424.

[17] M. Michielsen, M. K. Vanhees, and F. Verstreken, *Three-dimensional planning and surgical guidance of malunion correction,* in *Distal Radius Fractures, Evidence Based Managament* (Elsevier, 2021) pp. 341–350.

[18] F. Carrillo, L. Vlachopoulos, A. Schweizer, L. Nagy, J. Snedeker, and P. Fürnstahl, *A time saver: Optimization approach for the fully automatic 3d planning of forearm osteotomies,* (2017).

[19] P. Fürnstahl, A. Schweizer, M. Graf, L. Vlachopoulos, S. Fucentese, S. Wirth, L. Nagy, G. Szekely, and O. Goksel, *Surgical treatment of long-bone deformities: 3d preoperative planning and patient-specific instrumentation,* in *Computational Radiology for Orthopaedic Interventions*, edited by G. Zheng and S. Li (Springer International Publishing, Cham, 2016) pp. 123–149.

[20] *Materialise 3-matic: Design optimization software,* https://www.materialise.com/en/industrial/software/3-matic, accessed: 2023-04-19.

[21] D. P. R. R, D. V. Gupta, D. R. Soni, D. A. Jha, and D. C. S. S. Reddy, *Radial bow- its importance in return of rotation after fixation of fracture both bones forearm in adult,* International Journal of Orthopaedics Sciences **4(4)**, 68 (2018).

[22] *Elbow and forearm,* https://www.kenhub.com/en/library/anatomy/elbow-and-forearm (2022), accessed: 2023-04-20.

[23] J. T. Helms and B. B. Kenia A. Maldonado, *Anatomy, Shoulder and Upper Limb, Hand Radiocarpal Joint* (StatPearls Publishing, 2022).

[24] J. C. McGinley and S. H. Kozin, *Interosseous membrane anatomy and functional mechanics.* Clinical Orthopaedics and Related Research **383**, 108 (2001).

[25] *Elbow > bones,* https://sites.google.com/site/msklearnp/elbow/bones (2022), accessed: 2023-04-20.

[26] *Movements muscles of radioulnar joint,* https://www.youtube.com/watch?v=L4VN67kFaLQ (2023), accessed: 2023-04-26.

[27] L. Nagy, L. Jankauskas, and C. E. Dumont, *Correction of forearm malunion guided by the preoperative complaint.* Clinical Orthopaedics and Related Research **466(6)**, 1419–1428 (2008).

[28] E. H. Schemitsch and R. R. Richards, *The effect of malunion on functional outcome after plate fixation of fractures of both bones of the forearm in adults,* The Journal of bone and joint surgery **74(7)**, 1068–1078 (1992).

[29] K. Rathnayaka, K. I. Momot, H. Noser, A. Volp, M. A. Schuetz, T. Sahama, and B. Schmutz, *Quantification of the accuracy of mri generated 3d models of long bones compared to ct generated 3d models,* Medical Engineering Physics **34**, 357 (2012).

[30] *Most popular programming languages for automation,* https://careerkarma.com/blog/best-programming-languages-for-automation/ (), accessed: 2023-05-18.

[31] *What is automation?* https://www.ibm.com/topics/automation (), accessed: 2023-05-18.

[32] *optimization,* https://dictionary.cambridge.org/dictionary/english/optimization (2023), accessed: 2023-04-28.

[33] *optimization,* https://www.britannica.com/science/optimization (2023), accessed: 2023-04-28.

[34] *Iii. search space,* https://courses.cs.washington.edu/courses/cse473/06sp/GeneticAlgDemo/searchs.html (1998), accessed: 2023-04-30.

[35] *How to choose an optimization algorithm,* https://machinelearningmastery.com/tour-of-optimization-algorithms/ (2023), accessed: 2023-04-28.

[36] *Ct hand and wrist (protocol),* https://radiopaedia.org/articles/ct-hand-and-wrist-protocol-1 (2023), accessed: 2023-04-26.

[37] G. Wu, F. C. van der Helm, H. (DirkJan) Veeger, M. Makhsous, P. Van Roy, C. Anglin, J. Nagels, A. R. Karduna, K. McQuade, X. Wang, F. W. Werner, and B. Buchholz, *Isb recommendation on definitions of joint coordinate systems of various joints for the reporting of human joint motion—part ii: shoulder, elbow, wrist and hand,* Journal of Biomechanics **38**, 981 (2005).

[38] *Iterative closest point (icp) and other registration algorithms□,* https://docs.mrpt.org/reference/latest/tutorial-icp-alignment.html (2023), accessed: 2023-04-26.

[39] *Global registration,* http://www.open3d.org/docs/0.7.0/tutorial/Advanced/global_registration.html#global-registration (2018), accessed: 08-03-2023.

[40] M. A. Audette, F. P. Ferrie, and T. M. Peters, *An algorithmic overview of surface registration techniques for medical imaging,* Medical Image Analysis **4**, 201 (2000).

[41] X. Yu and M. Gen, *Introduction to Evolutionary Algorithms* (Springer) pp. 5–10.

[42] T. Bartz-Beielstein, J. Branke, J. Mehnen, and O. Mersmann, *Evolutionary algorithms,* WIREs data mining and knowledge discovery **4(3)**, 178 (2014).

[43] S. Bhattacharyya and G. J. Koehler, *An analysis of non-binary genetic algorithms with cardinality 2,* Complex Systems **8**, 227 (1994).

[44] *evolutionary algorithm,* https://towardsdatascience.com/introduction-to-evolutionary-algorithms-a8594b48 (2018), accessed: 2023-04-29.

[45] *Genetic algorithm key terms, explained,* https://www.kdnuggets.com/2018/04/genetic-algorithm-key-terms-explained.html (2022), accessed: 22-03-2023.

[46] C.-W. Bong and R. Mandava, *Multiobjective optimization approaches in image segmentation – the directions and challenges,* International Journal of Advances in Soft Computing and Its Applications **2** (2010).

[47] *Mse vs. rmse: Which metric should you use?* https://www.statology.org/mse-vs-rmse/ (2021), accessed: 24-03-2023.

[48] D. van Loon, *Forearm rotation after malunited diaphyseal fracture: Predicting range of motion with a kinematic model,* (2022), http://resolver.tudelft.nl/uuid:0e5acbe1-c55f-4b15-a781-0ac249130e27.

[49] H. Maaranen, K. Miettinen, and M. Mäkelä, *Quasi-random initial population for genetic algorithms,* Computers Mathematics with Applications **47**, 1885 (2004).

[50] *A simple hack to boost any global optimization algorithm,* https://towardsdatascience.com/a-simple-hack-to-boost-any-global-optimization-algorithm-bdea461b87 (2021), accessed: 22-03-2023.

[51] *haltonset,* https://www.mathworks.com/help/stats/haltonset.html (2023), accessed: 2023-05-22.

[52] *Introduction to constrained optimization,* https://web.stanford.edu/group/sisl/k12/optimization/MO-unit3-pdfs/3.1introandgraphical.pdf, accessed: 2023-04-29.

[53] J. G. Dobbe, K. J. D. Pré, P. Kloen, L. Blankevoort, and G. J. Streekstra, *Computer-assisted and patient-specific 3-d planning and evaluation of a single-cut rotational osteotomy for complex long-bone deformities,* Medical and Biological Engineering and Computing **49** (2011), 10.1007/s11517-011-0830-3.

[54] *Tournament selection (ga),* https://www.geeksforgeeks.org/tournament-selection-ga/ (2022), accessed: 16-03-2023.

[55] T. Blickle and L. Thiele, *A Comparison of Selection Schemes Used in Evolutionary Algorithms,* Evolutionary Computation **4**, 361 (1996), https://direct.mit.edu/evco/article-pdf/4/4/361/1492921/evco.1996.4.4.361.pdf .

[56] A. Shukla, H. M. Pandey, and D. Mehrotra, *Comparative review of selection techniques in genetic algorithm,* in *2015 International Conference on Futuristic Trends on Computational Analysis and Knowledge Management (ABLAZE)* (2015) pp. 515–519.

[57] N. García-Pedrajas, C. Martínez, and D. Ortiz-Boyer, *Cixl2: A crossover operator for evolutionary algorithms based on population features,* Journal of Global Optimization **24** (2011), 10.1613/jair.1660.

[58] A. Eiben, R. Hinterding, and Z. Michalewicz, *Parameter control in evolutionary algorithms,* IEEE Transactions on Evolutionary Computation **3**, 124 (1999).

[59] *Genetic algorithms: Crossover probability and mutation probability,* https://www.baeldung.com/cs/genetic-algorithms-crossover-probability-and-mutation-probability (2023), accessed: 14-03-2023.

[60] *Mutation algorithms for string manipulation (ga),* https://www.geeksforgeeks.org/mutation-algorithms-for-string-manipulation-ga/ (2022), accessed: 13-03-2023.

[61] A. Rogers and A. Prugel-Bennett, *Genetic drift in genetic algorithm selection schemes,* IEEE TRANSACTIONS ON EVOLUTIONARY COMPUTATION **3**, 298 (1999).

[62] G. Dick and P. Whigham, *The behaviour of genetic drift in a spatially-structured evolutionary algorithm,* in *2005 IEEE Congress on Evolutionary Computation*, Vol. 2 (2005) pp. 1855–1860 Vol. 2.

[63] H. Du, Z. Wang, W. Zhan, and J. Guo, *Elitism and distance strategy for selection of evolutionary algorithms,* IEEE Access **6**, 44531 (2018).

[64] *Types of reliability,* https://conjointly.com/kb/types-of-reliability/ (2023), accessed: 2023-05-03.

[65] V. Toğan and A. T. Daloğlu, *An improved genetic algorithm with initial population strategy and self-adaptive member grouping,* Computers Structures **86**, 1204 (2008).

[66] F. Ambellan, H. Lamecker, C. von Tycowicz, and S. Zachow, *Statistical shape models: Understanding and mastering variation in anatomy,* Advances in experimental medicine and biology , 67–84 (2019).

[67] L. Vlachopoulos, M. Lüthi, F. Carrillo, C. Gerber, G. Székely, and P. Fürnstahl, *Restoration of the patient-specific anatomy of the proximal and distal parts of the humerus: Statistical shape modeling versus contralateral registration method,* The Journal of bone and joint surgery **100** (2018), https://doi.org/10.2106/JBJS.17.00829.

[68] S. K. Smit and A. E. Eiben, *Using entropy for parameter analysis of evolutionary algorithms,* in *Experimental Methods for the Analysis of Optimization Algorithms*, edited by T. Bartz-Beielstein, M. Chiarandini, L. Paquete, and M. Preuss (Springer Berlin Heidelberg, Berlin, Heidelberg, 2010) pp. 287–310.

[69] A. Hassanat, K. Almohammadi, E. Alkafaween, E. Abunawas, A. Hammouri, and V. B. S. Prasath, *Choosing mutation and crossover ratios for genetic algorithms—a review with a new dynamic approach,* Information **10** (2019), 10.3390/info10120390.

[70] M. Bhattacharya, *Diversity handling in evolutionary landscape,* Proceedings of the International Workshop on Combinations of Intelligent Methods and Applications , 1 (2014).

[71] B. Rajakumar and A. George, *Apoga: An adaptive population pool size based genetic algorithm,* AASRI Procedia **4**, 288 (2013), 2013 AASRI Conference on Intelligent Systems and Control.

[72] O. M. Shir, *Niching in evolutionary algorithms,* in *Handbook of Natural Computing*, edited by G. Rozenberg, T. Bäck, and J. N. Kok (Springer Berlin Heidelberg, Berlin, Heidelberg, 2012) pp. 1035–1069.

[73] *What is robustness,* https://www.igi-global.com/dictionary/robustness/25481 (2023), accessed: 2023-05-05.

Appendices contents

A

Osteotomy plans

Table A.1: Degree of deformity of each patient case

	rotation$_x$ (°)	**rotation$_y$ (°)**	**rotation$_z$ (°)**	**translation$_x$ (mm)**	**translation$_y$ (mm)**	**translation$_z$ (mm)**
Pt1	-14.40	4.76	7.27	2.60	6.40	-2.66
Pt2	-15.03	1.55	16.73	-1.67	1.56	-1.42
Pt3	9.54	1.31	-14.64	1.92	-3.68	1.82
Pt4	22.24	6.40	14.90	9.95	-12.26	-7.08
Pt5	17.80	1.67	-13.30	-1.74	-13.81	-4.03
Pt6	26.93	9.13	27.77	6.49	-5.87	-6.66
Pt7	3.96	-10.96	-0.54	-1.32	-1.76	0.17
Pt8	7.31	13.43	-46.64	1.74	-11.39	-2.34
Pt9	14.62	0.19	-1.98	-1.01	-3.33	-1.08
Pt10	22.11	19.20	-8.33	10.68	-17.04	-13.25
Pt11	-19.49	11.40	12.07	7.41	15.84	-7.63
Pt12	4.57	-2.32	-40.69	-3.77	-7.27	-1.00
Pt13	-3.54	9.16	14.05	6.76	0.19	-0.92
Pt14	-7.63	-4.32	0.68	3.13	0.73	-1.65
Pt15	-7.68	-5.72	1.62	4.82	-5.45	-0.86

Table A.2: Patient cases excluded before validation due to no bone contact

Patient case	**Alignment %**
1	15, 25
2	15
3	15, 25
4	15, 25
5	15
6	15, 25
8	15, 25
9	15
10	15
11	15, 25

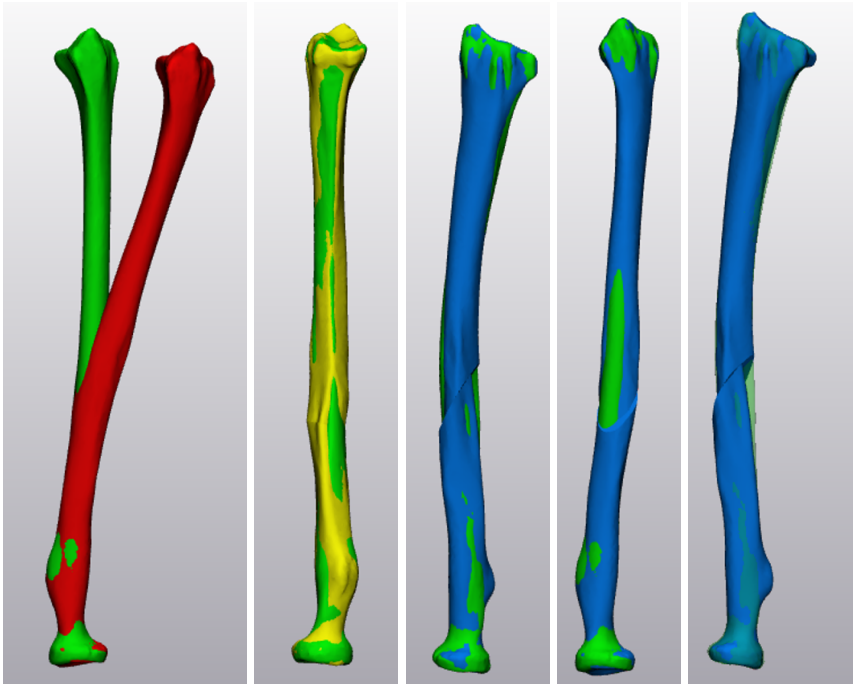

(a) (b) (c) (d) (e)

Figure A.1: Patient case 1, alignment 100%. *Red = pathological bone proximally aligned, yellow = planning by Materialise, blue = pathological bone, green = reference bone.*

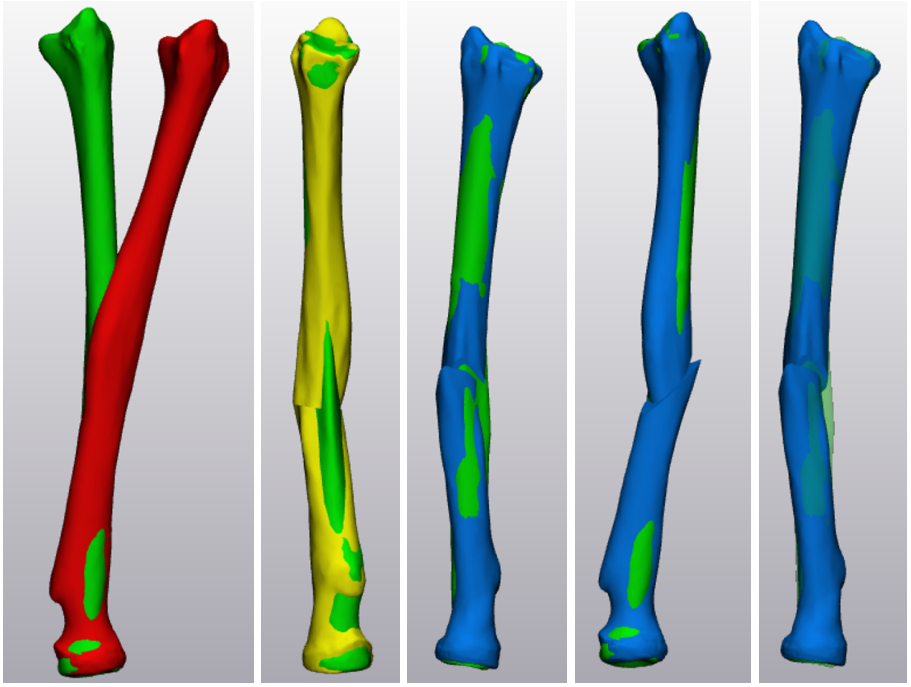

(a) (b) (c) (d) (e)

Figure A.2: Patient case 2, alignment 100%. *Red = pathological bone proximally aligned, yellow = planning by Materialise, blue = pathological bone, green = reference bone.*

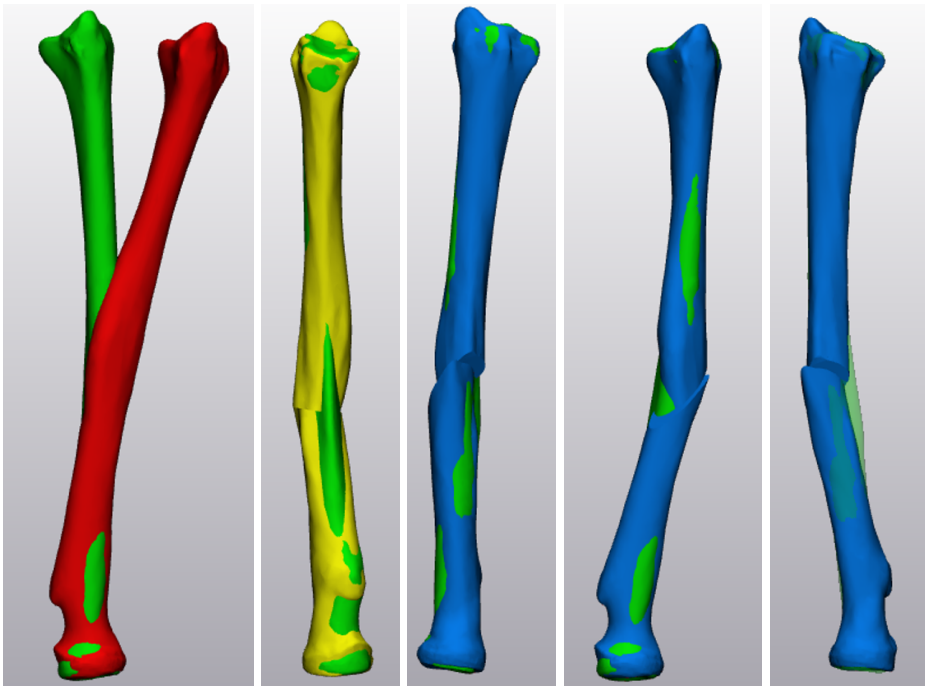

(a) (b) (c) (d) (e)

Figure A.2: Patient case 2, alignment 25%. *Red = pathological bone proximally aligned, yellow = planning by Materialise, blue = pathological bone, green = reference bone.*

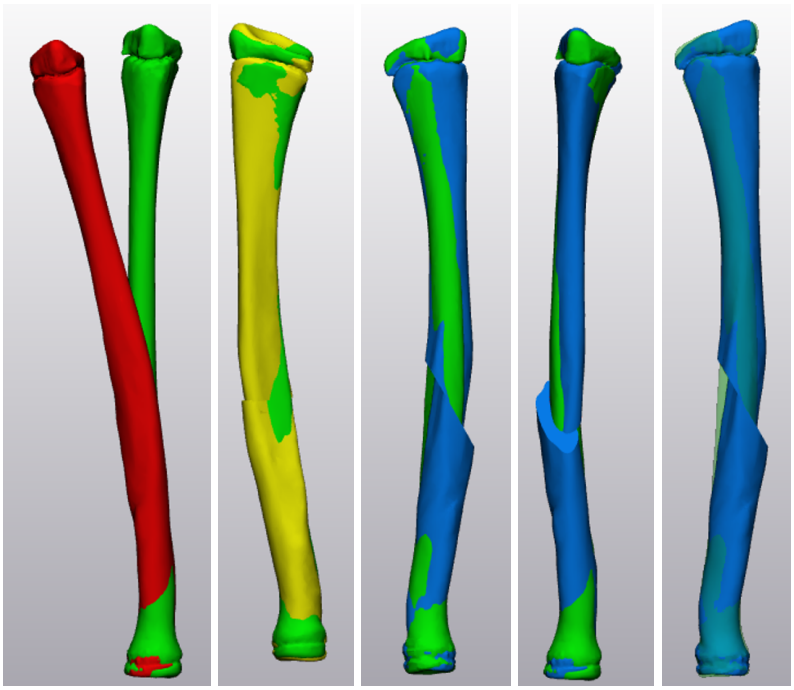

(f) (g) (h) (i) (j)

Figure A.3: Patient case 3, alignment 100%. *Red = pathological bone proximally aligned, yellow = planning by Materialise, blue = pathological bone, green = reference bone.*

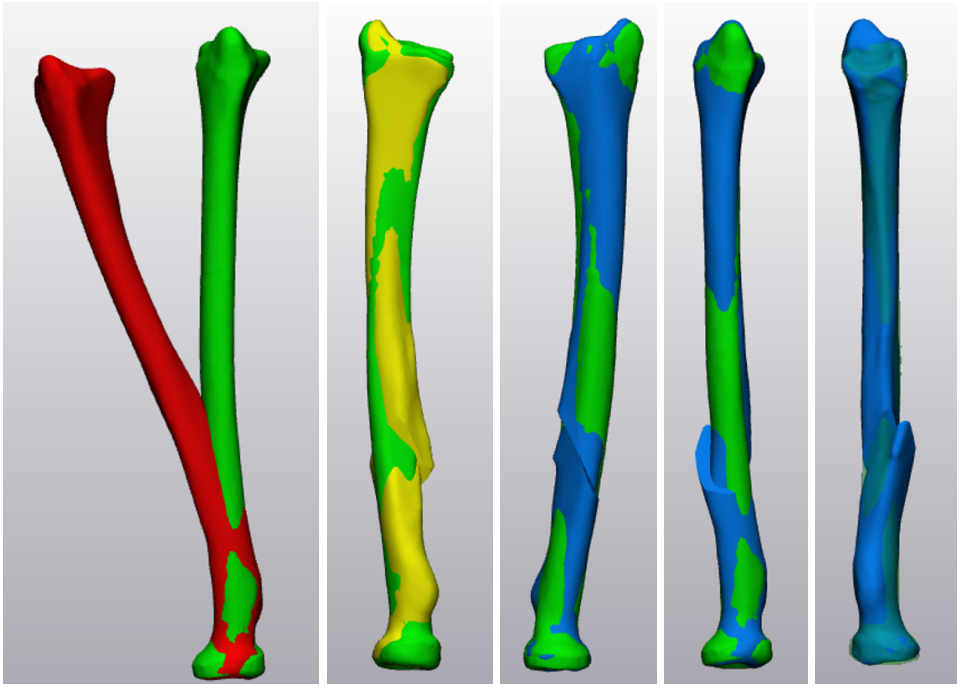

(a) (b) (c) (d) (e)

Figure A.4: Patient case 4, alignment 100%. *Red = pathological bone proximally aligned, yellow = planning by Materialise, blue = pathological bone, green = reference bone.*

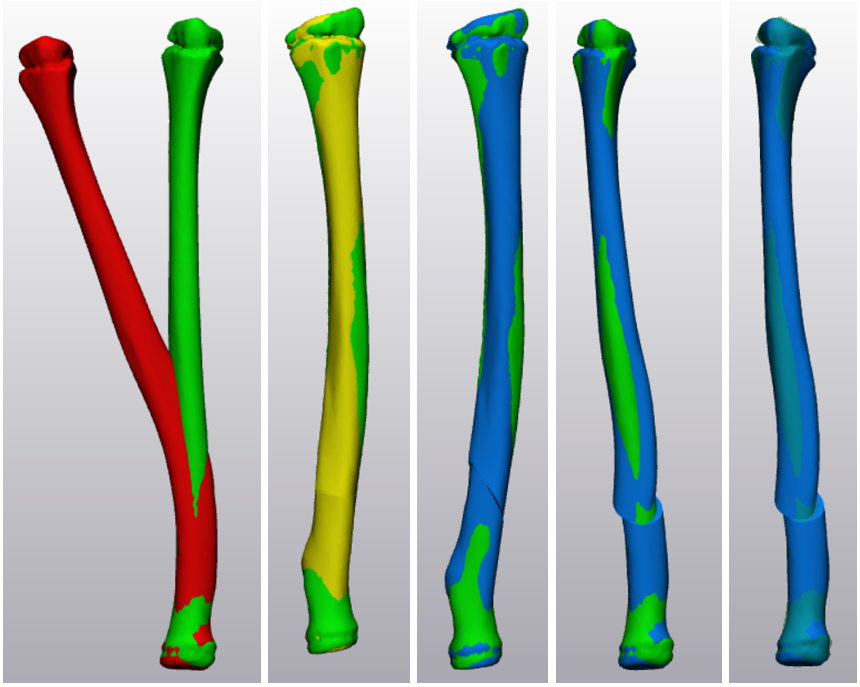

(a) (b) (c) (d) (e)

Figure A.5: Patient case 5, alignment 100%. *Red = pathological bone proximally aligned, yellow = planning by Materialise, blue = pathological bone, green = reference bone.*

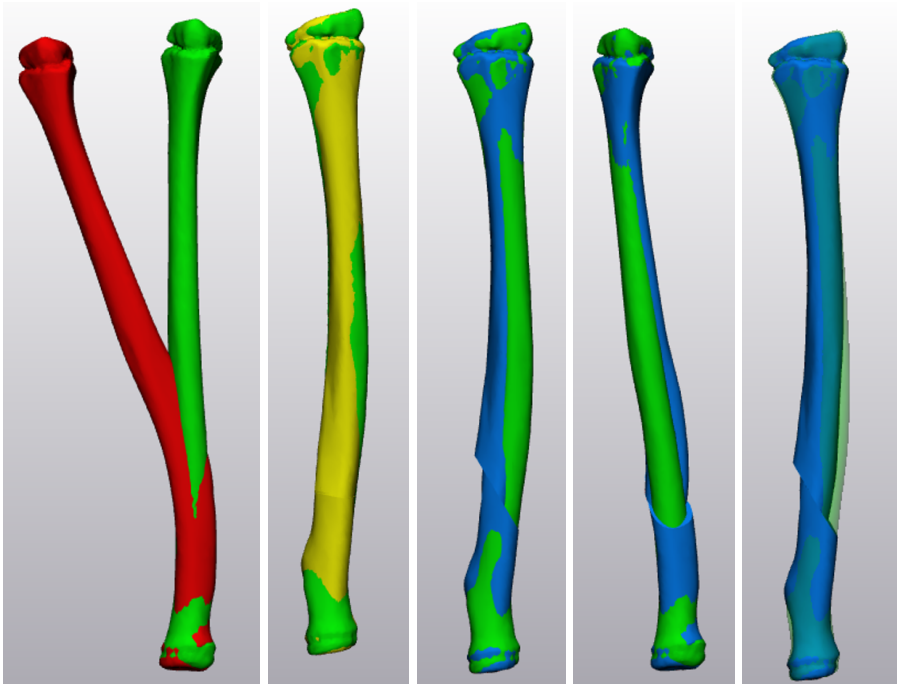

(a) (b) (c) (d) (e)

Figure A.5: Patient case 5, alignment 25%. *Red = pathological bone proximally aligned, yellow = planning by Materialise, blue = pathological bone, green = reference bone.*

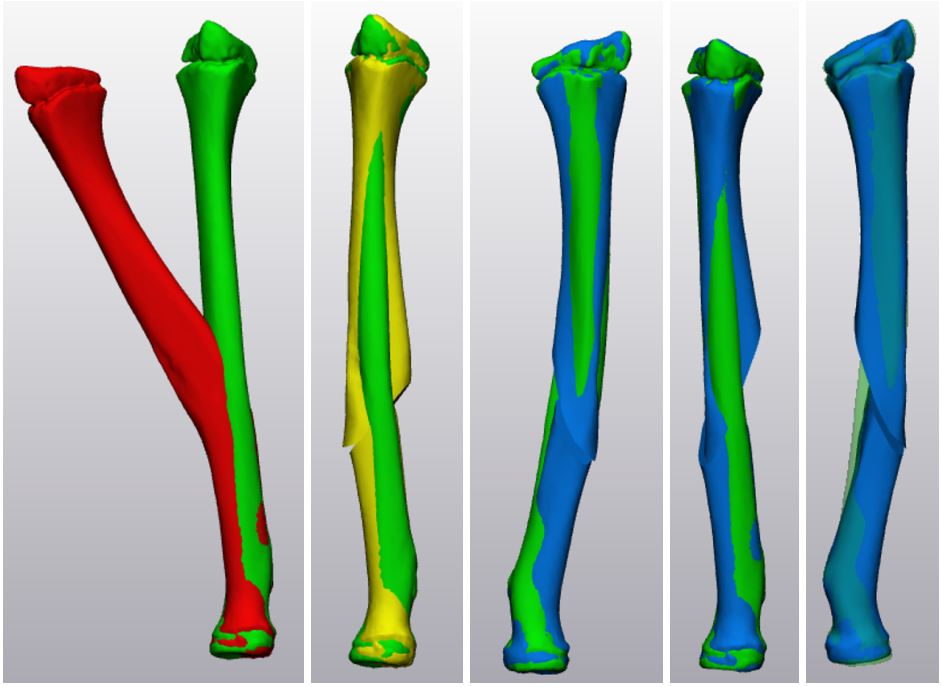

(f) (g) (h) (i) (j)

Figure A.6: Patient case 6, alignment 100%. *Red = pathological bone proximally aligned, yellow = planning by Materialise, blue = pathological bone, green = reference bone.*

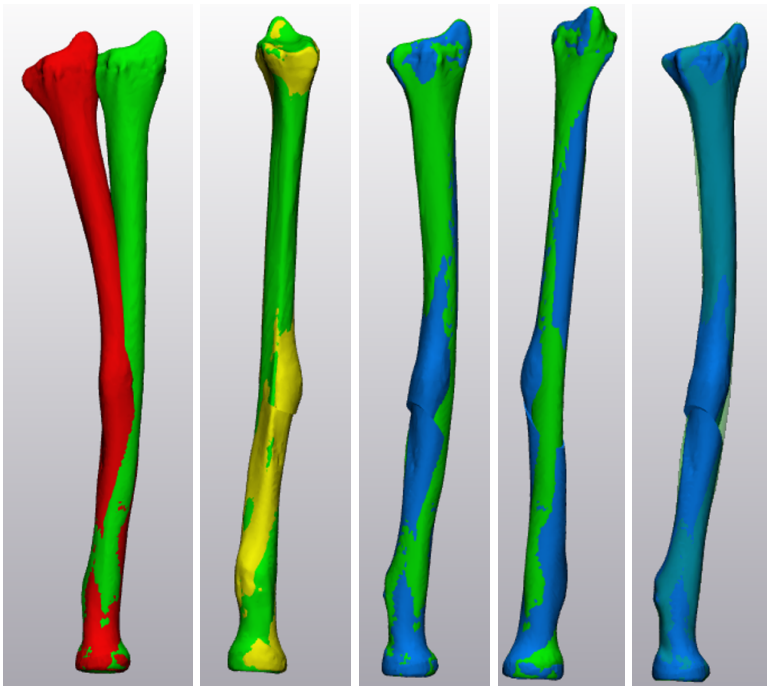

(a) (b) (c) (d) (e)

Figure A.7: Patient case 7, alignment 100%. *Red = pathological bone proximally aligned, yellow = planning by Materialise, blue = pathological bone, green = reference bone.*

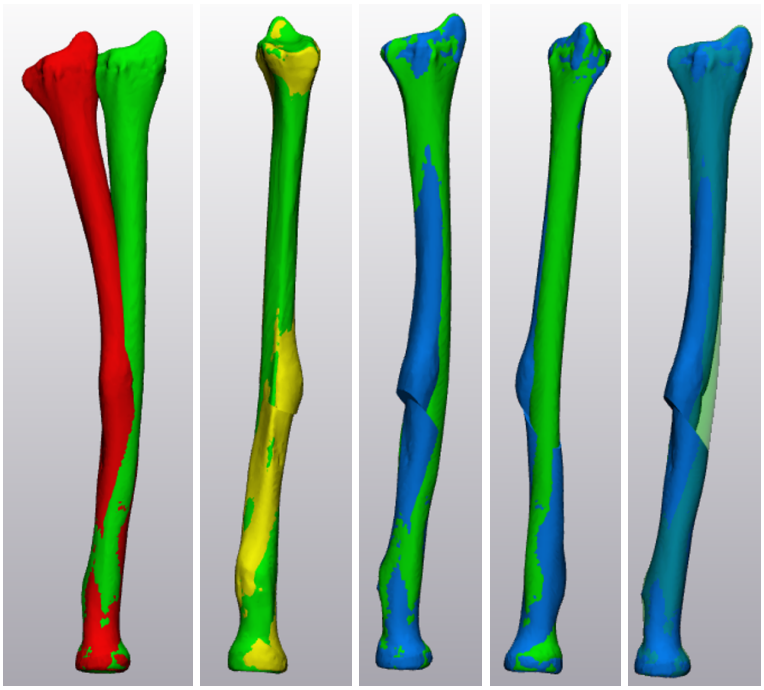

(a) (b) (c) (d) (e)

Figure A.7: Patient case 7, alignment 25%. *Red = pathological bone proximally aligned, yellow = planning by Materialise, blue = pathological bone, green = reference bone.*

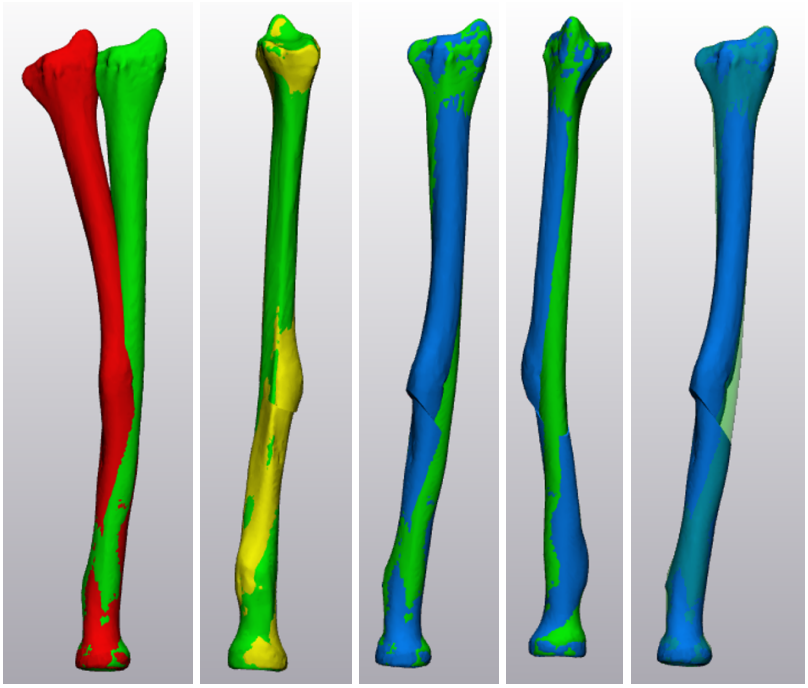

(f) (g) (h) (i) (j)

Figure A.7: Patient case 7, alignment 15%. *Red = pathological bone proximally aligned, yellow = planning by Materialise, blue = pathological bone, green = reference bone.*

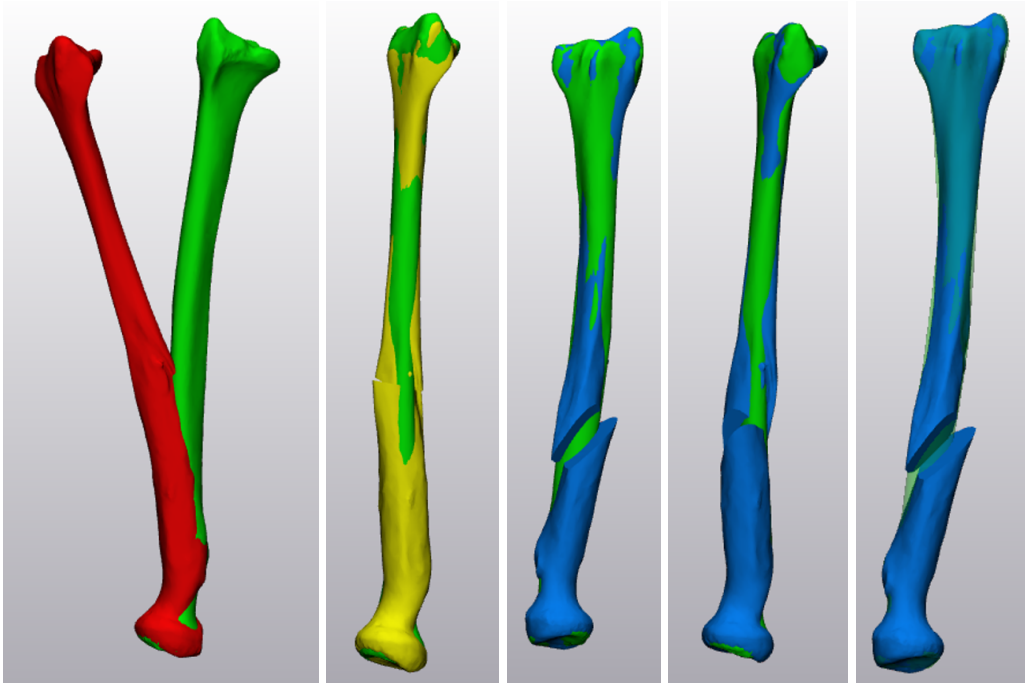

(k) (l) (m) (n) (o)

Figure A.8: Patient case 8, alignment 100%. *Red = pathological bone proximally aligned, yellow = planning by Materialise, blue = pathological bone, green = reference bone.*

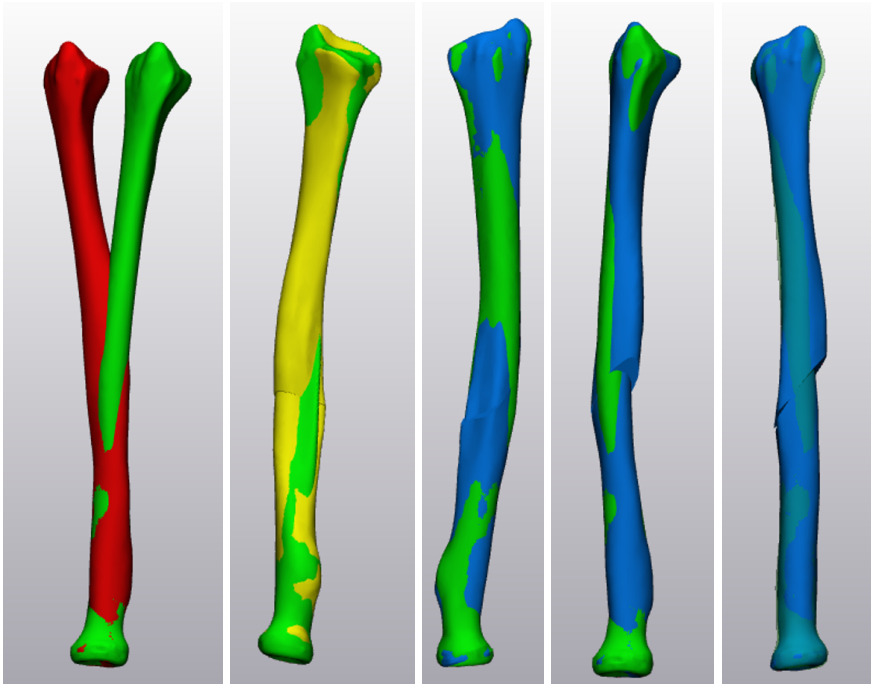

(a) (b) (c) (d) (e)

Figure A.9: Patient case 9, alignment 100%. *Red = pathological bone proximally aligned, yellow = planning by Materialise, blue = pathological bone, green = reference bone.*

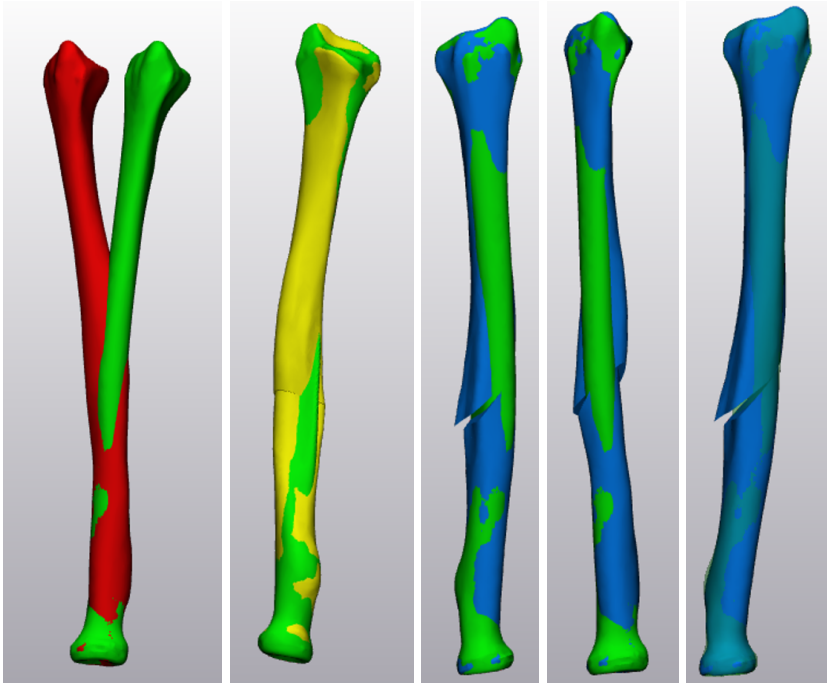

(a) (b) (c) (d) (e)

Figure A.9: Patient case 9, alignment 25%. *Red = pathological bone proximally aligned, yellow = planning by Materialise, blue = pathological bone, green = reference bone.*

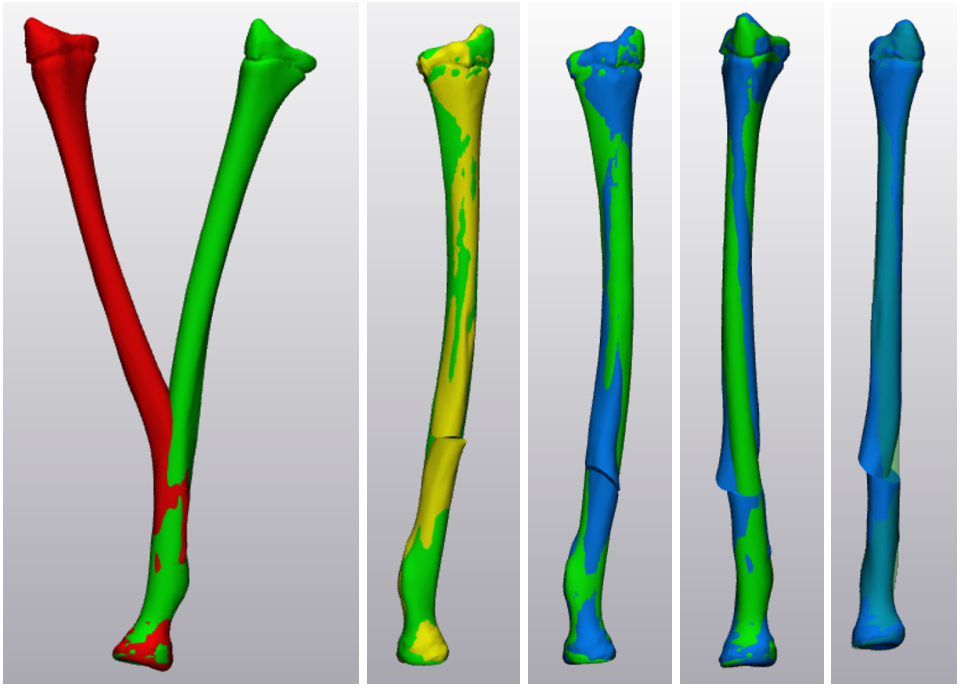

(f) (g) (h) (i) (j)

Figure A.10: Patient case 10, alignment 100%. *Red = pathological bone proximally aligned, yellow = planning by Materialise, blue = pathological bone, green = reference bone.*

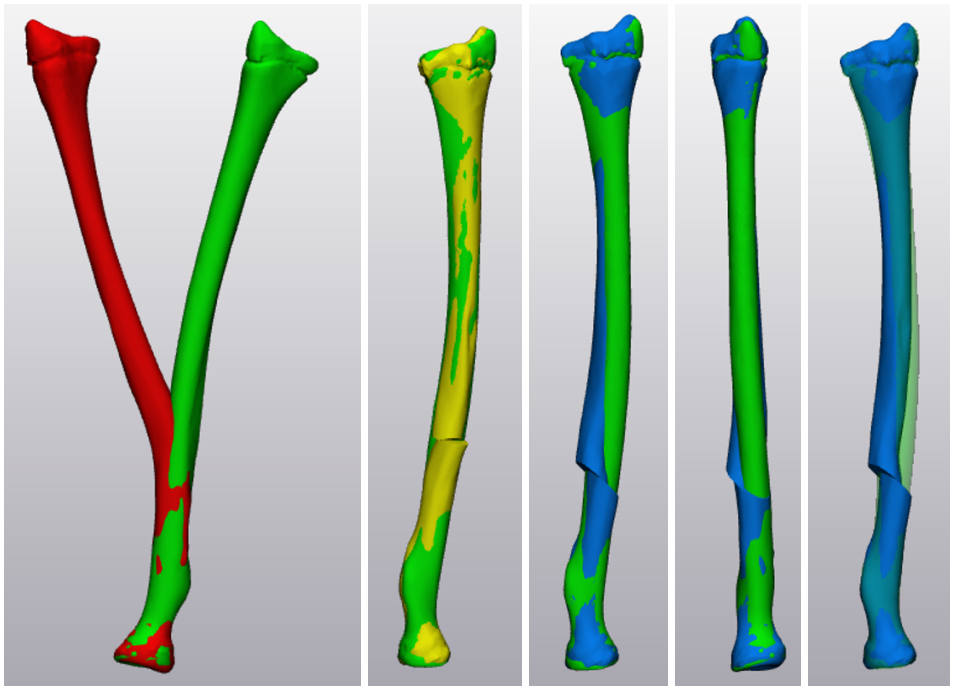

(a) (b) (c) (d) (e)

Figure A.10: Patient case 10, alignment 25%. *Red = pathological bone proximally aligned, yellow = planning by Materialise, blue = pathological bone, green = reference bone.*

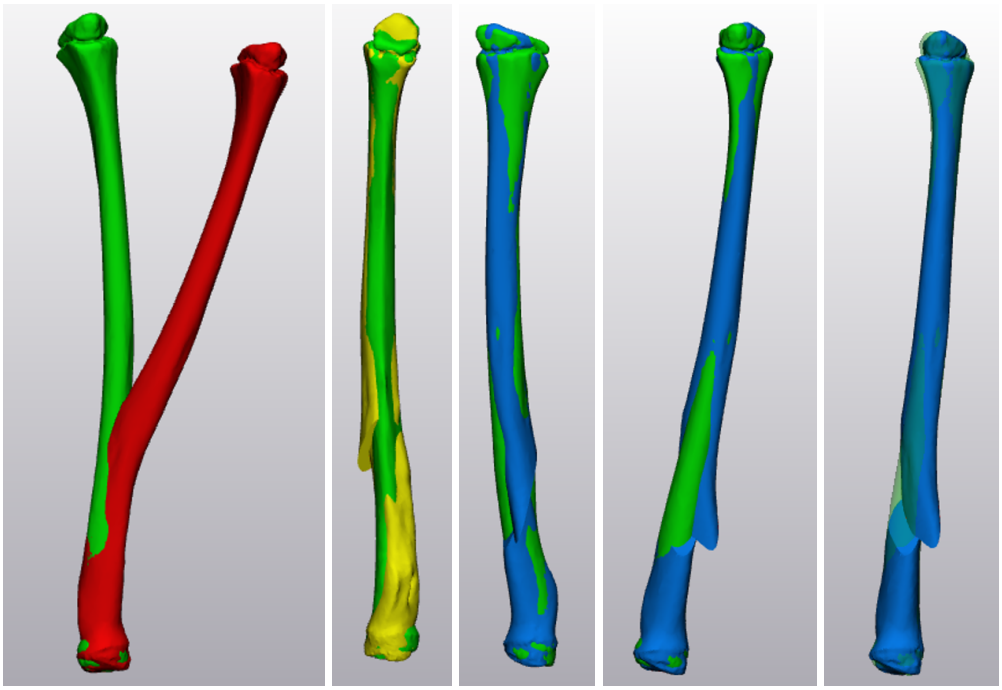

(f) (g) (h) (i) (j)

Figure A.11: Patient case 11, alignment 100%. *Red = pathological bone proximally aligned, yellow = planning by Materialise, blue = pathological bone, green = reference bone.*

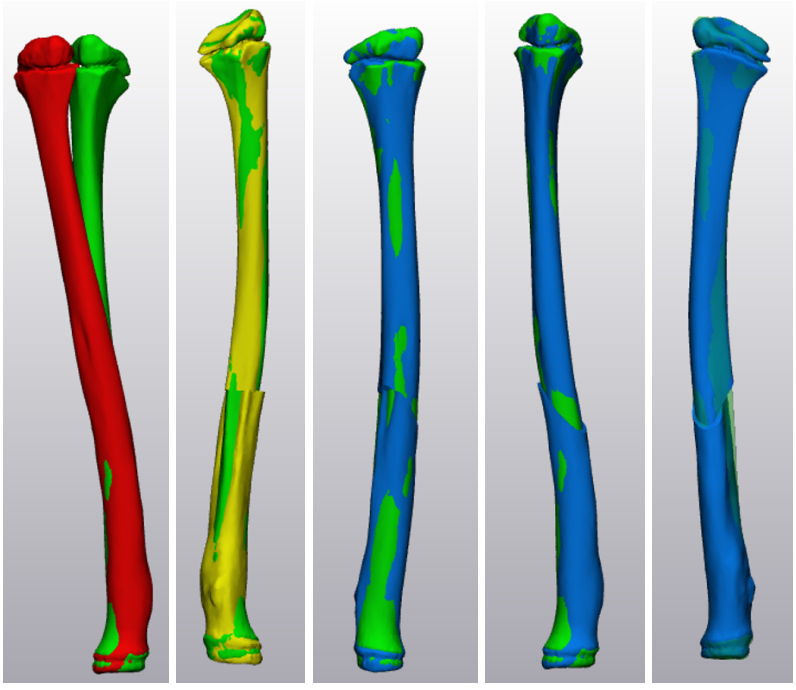

(a) (b) (c) (d) (e)

Figure A.12: Patient case 12, alignment 100%. *Red = pathological bone proximally aligned, yellow = planning by Materialise, blue = pathological bone, green = reference bone.*

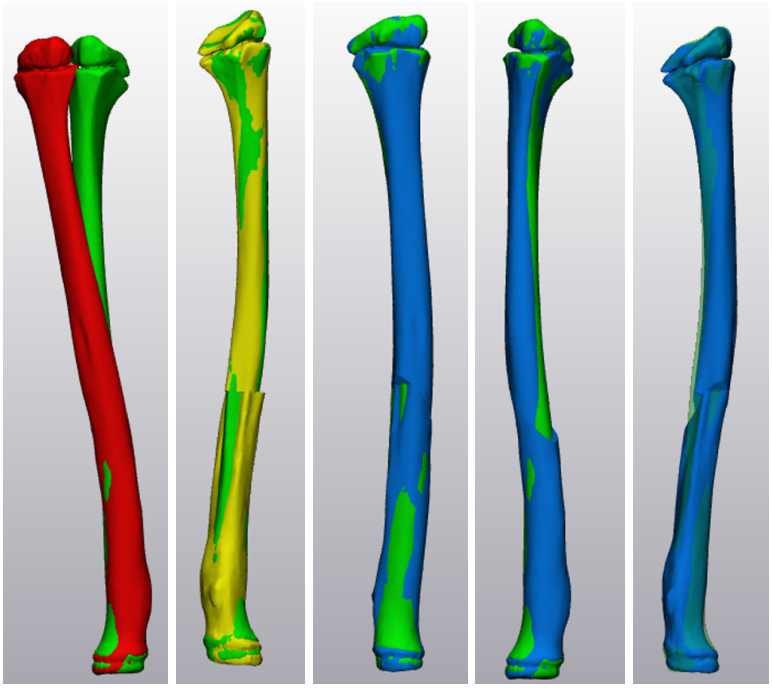

(a) (b) (c) (d) (e)

Figure A.12: Patient case 12, alignment 25%. *Red = pathological bone proximally aligned, yellow = planning by Materialise, blue = pathological bone, green = reference bone.*

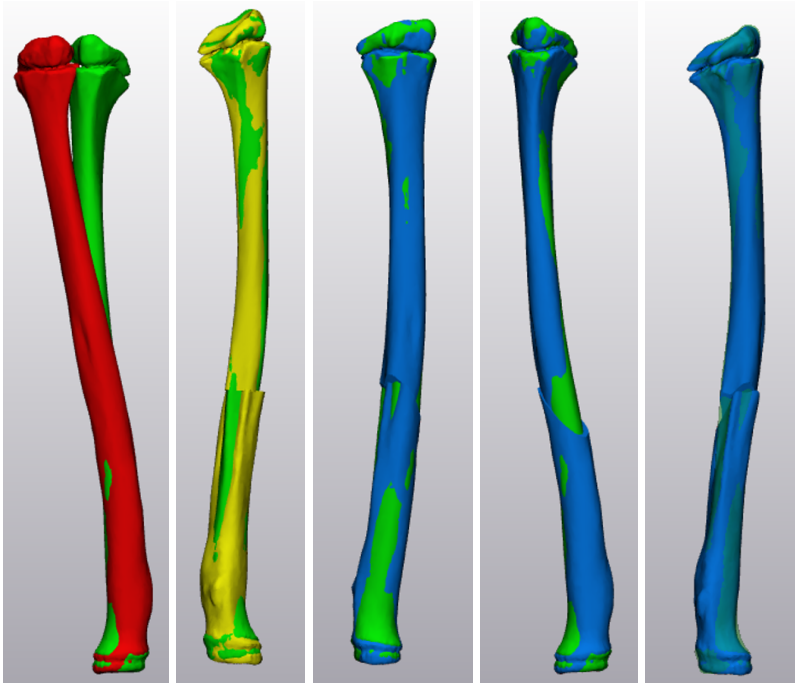

(f) (g) (h) (i) (j)

Figure A.12: Patient case 12, alignment 15%. *Red = pathological bone proximally aligned, yellow = planning by Materialise, blue = pathological bone, green = reference bone.*

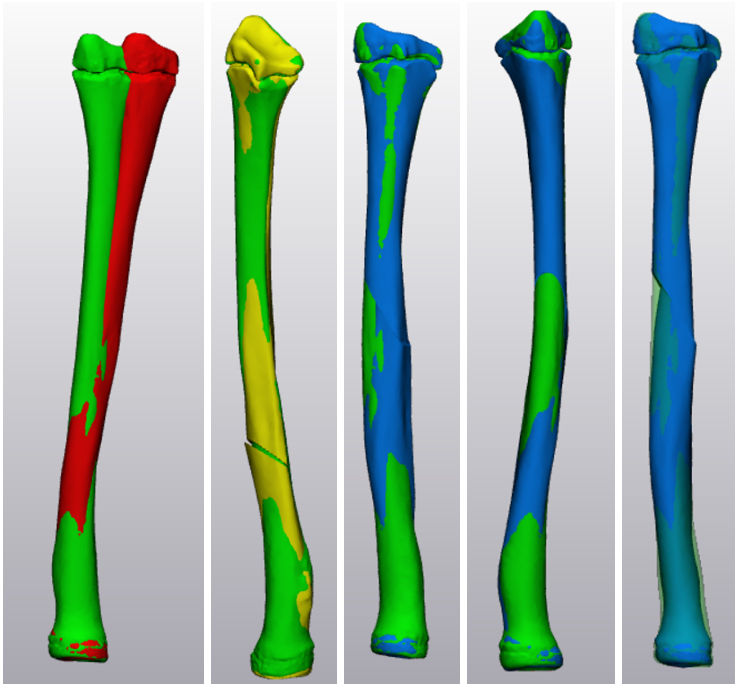

(k) (l) (m) (n) (o)

Figure A.13: Patient case 14, alignment 100%. *Red = pathological bone proximally aligned, yellow = planning by Materialise, blue = pathological bone, green = reference bone.*

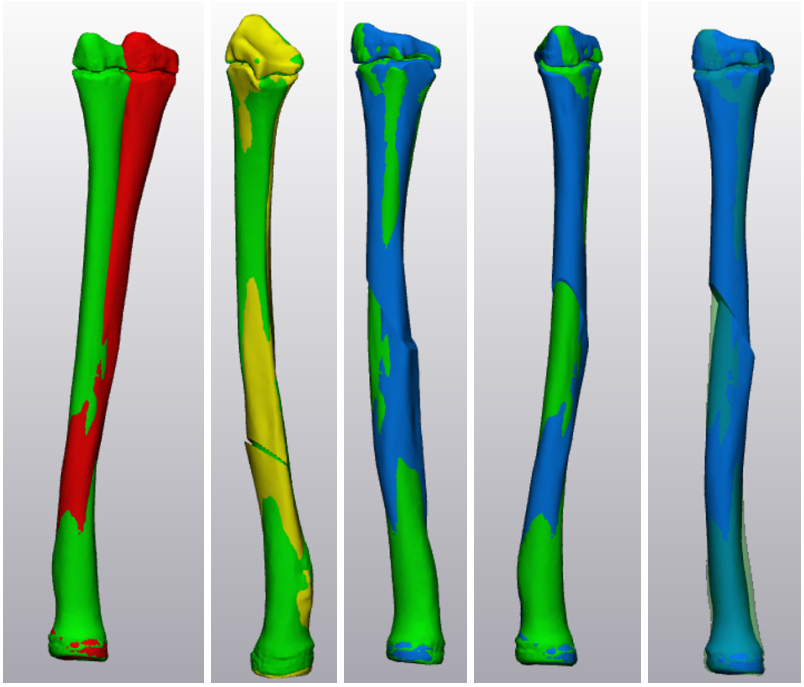

(a) (b) (c) (d) (e)

Figure A.13: Patient case 14, alignment 25%. *Red = pathological bone proximally aligned, yellow = planning by Materialise, blue = pathological bone, green = reference bone.*

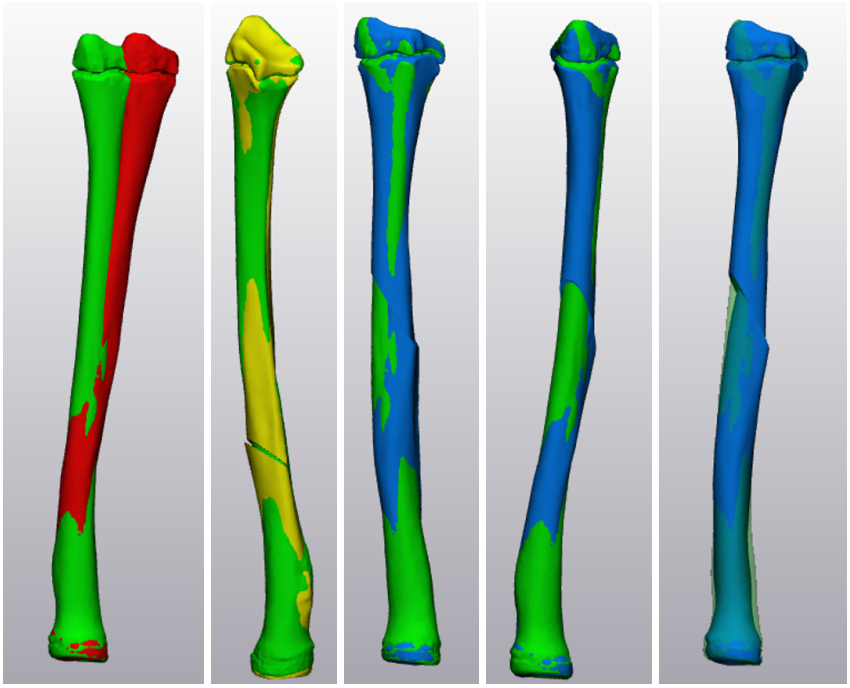

(f) (g) (h) (i) (j)

Figure A.13: Patient case 14, alignment 15%. *Red = pathological bone proximally aligned, yellow = planning by Materialise, blue = pathological bone, green = reference bone.*

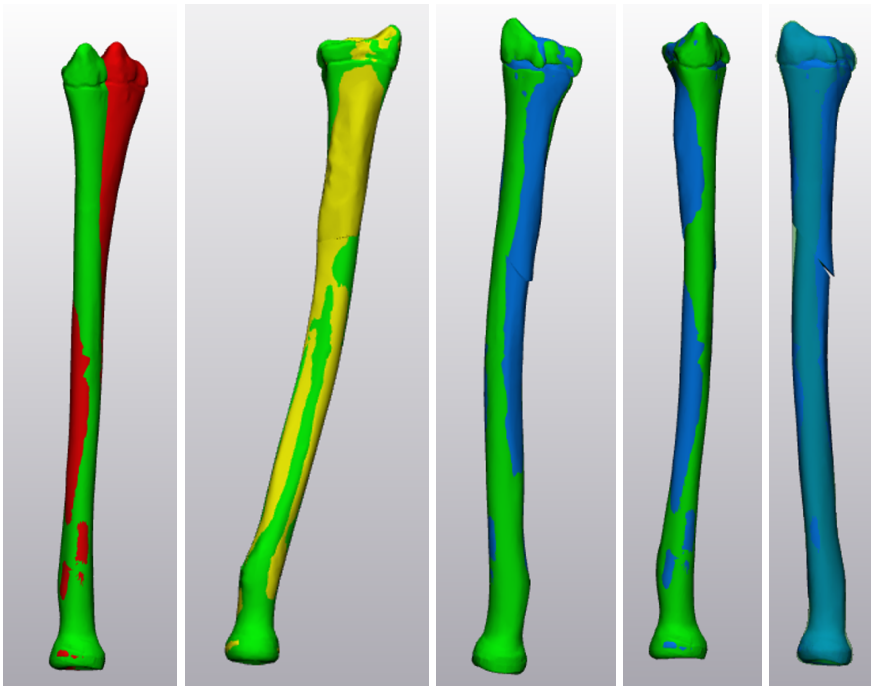

(k) (l) (m) (n) (o)

Figure A.14: Patient case 15, alignment 100%. *Red = pathological bone proximally aligned, yellow = planning by Materialise, blue = pathological bone, green = reference bone.*

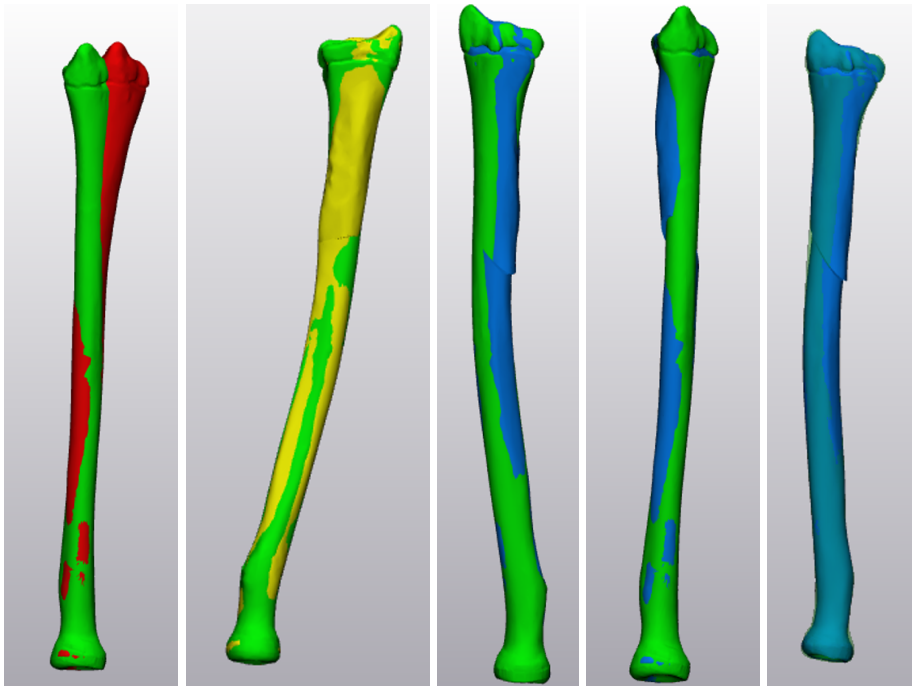

(a) (b) (c) (d) (e)

Figure A.14: Patient case 15, alignment 25%. *Red = pathological bone proximally aligned, yellow = planning by Materialise, blue = pathological bone, green = reference bone.*

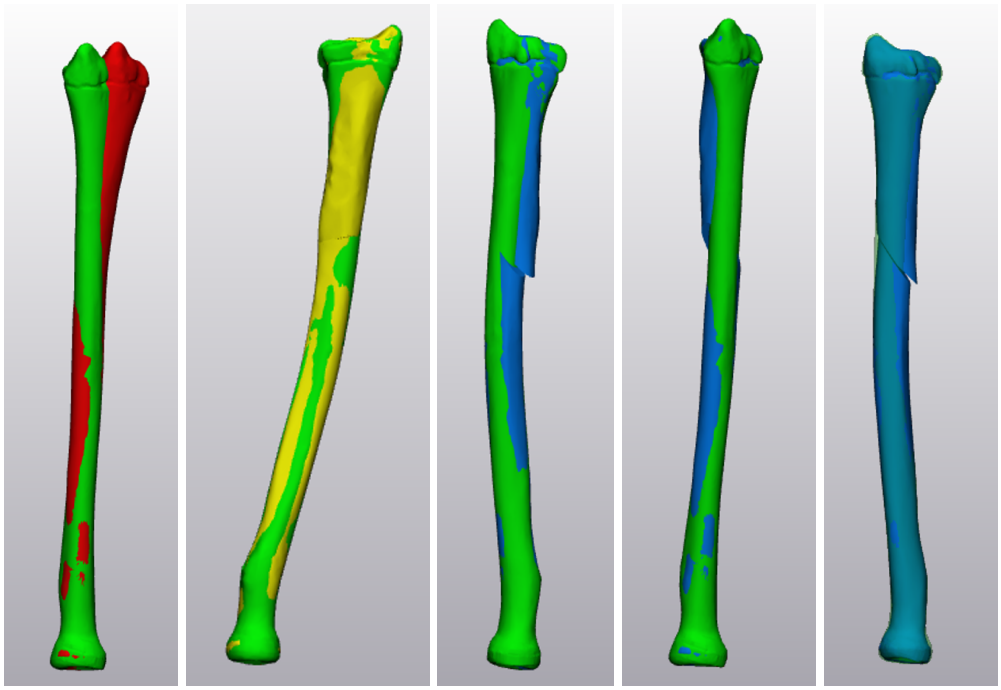

(f) (g) (h) (i) (j)

Figure A.14: Patient case 15, alignment 15%. *Red = pathological bone proximally aligned, yellow = planning by Materialise, blue = pathological bone, green = reference bone.*

B

BP score throughout optimization

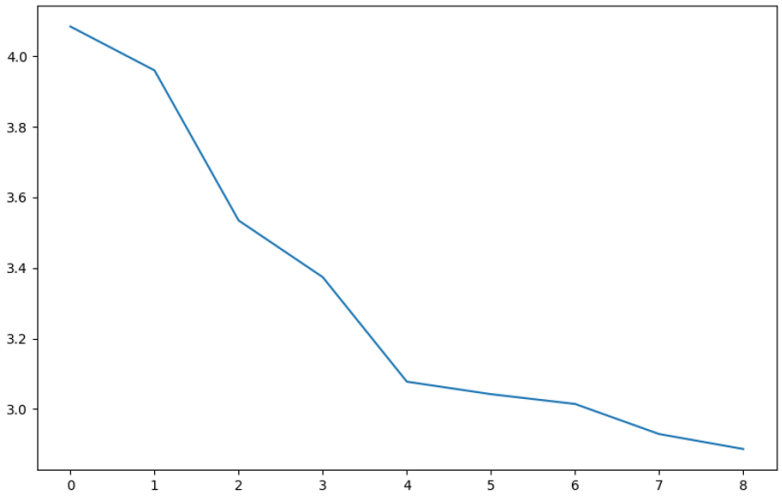

(a) Patient 1. Final BP score = 2.887, $\triangle$BP = 1.20

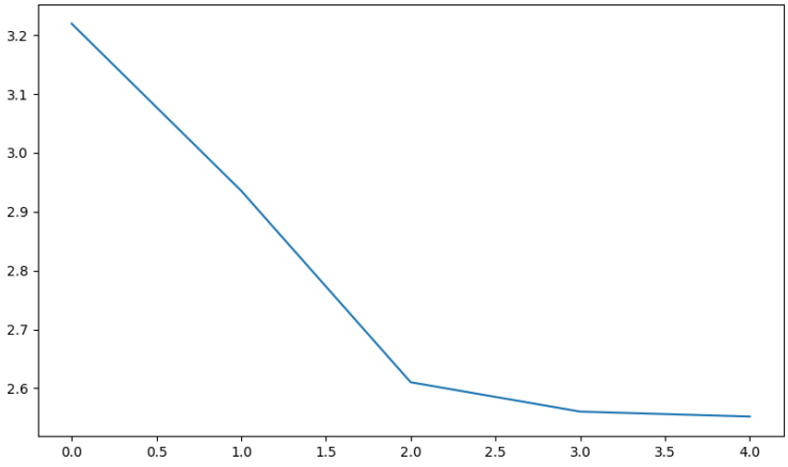

(b) Patient 2. Final BP score = 2.552, $\triangle$BP = 0.67

Figure B.1: Decrease in Bone Protrusion score throughout optimization.
y-axis = BP score, x-axis = incidence of decrease in BP

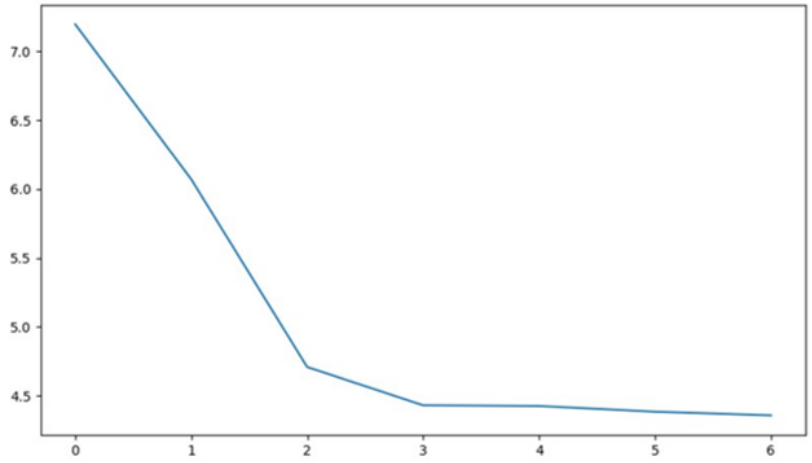

(a) Patient 3. Final BP score = 4.357, $\triangle$BP = 2.833

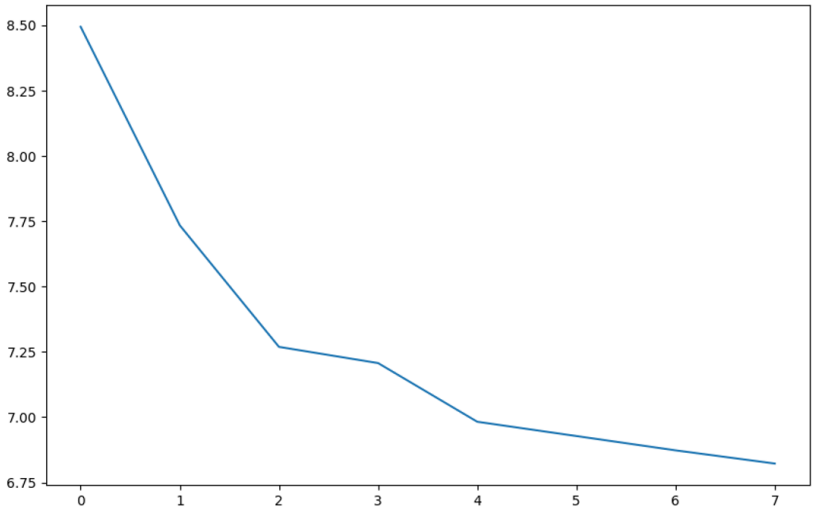

(b) Patient 4. Final BP score = 6.823, $\triangle$BP = 1.668

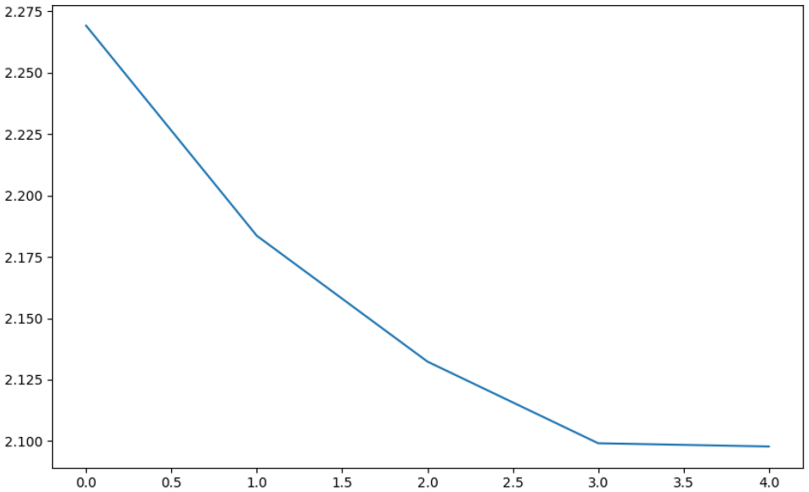

(c) Patient 5. Final BP score = 2.098, $\triangle$BP = 0.171

Figure B.1: Decrease in Bone Protrusion score throughout optimization.
y-axis = BP score, x-axis = incidence of decrease in BP

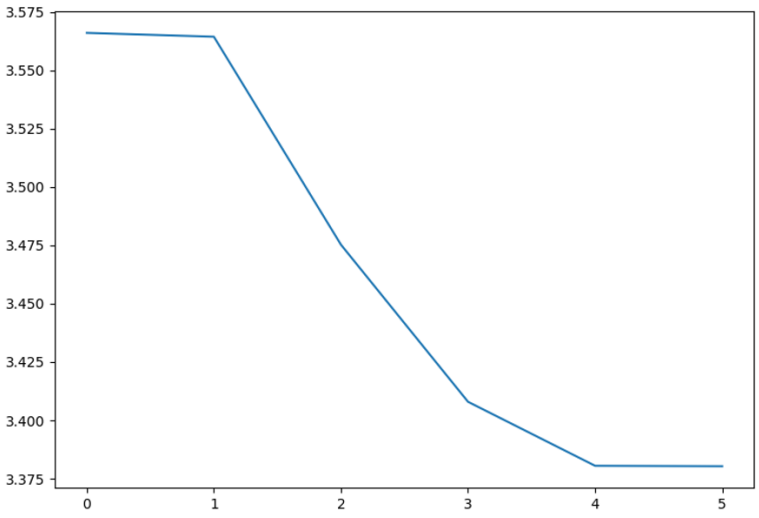

(d) Patient 6. Final BP score = 3.380, ∆BP = 0.186

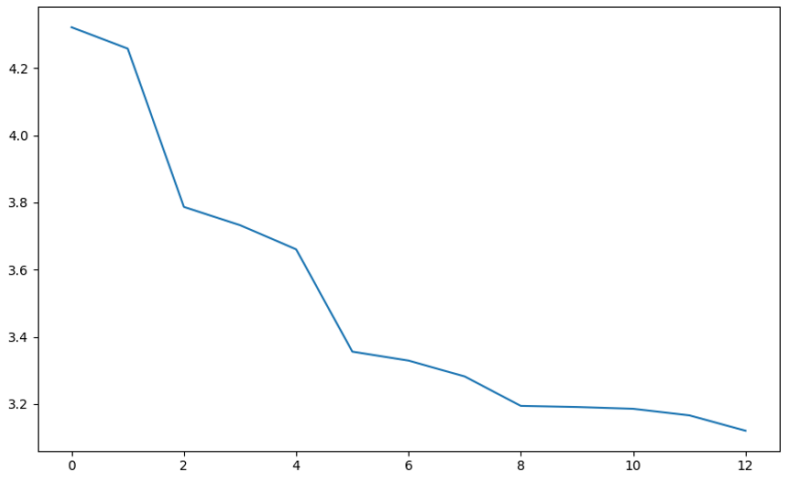

(e) Patient 7. Final BP score = 3.121, ∆BP = 1.202

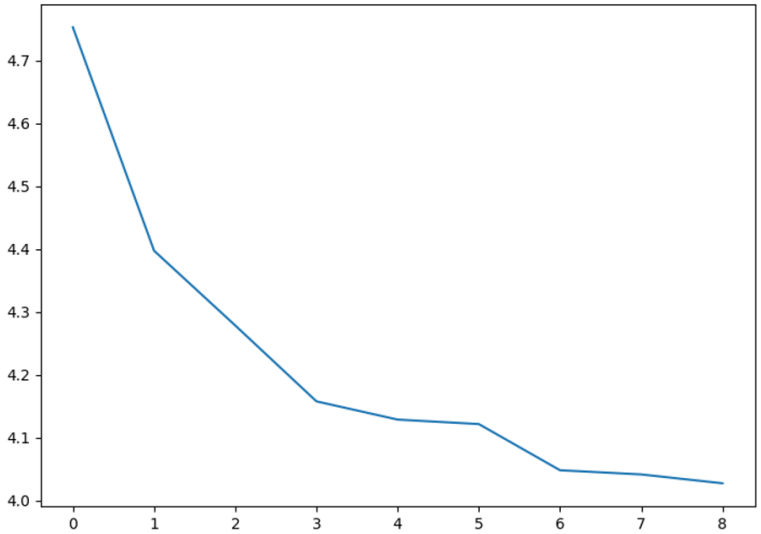

(f) Patient 8. Final BP score = 4.028, ∆BP = 0.725

Figure B.1: Decrease in Bone Protrusion score throughout optimization.
y-axis = BP score, x-axis = incidence of decrease in BP

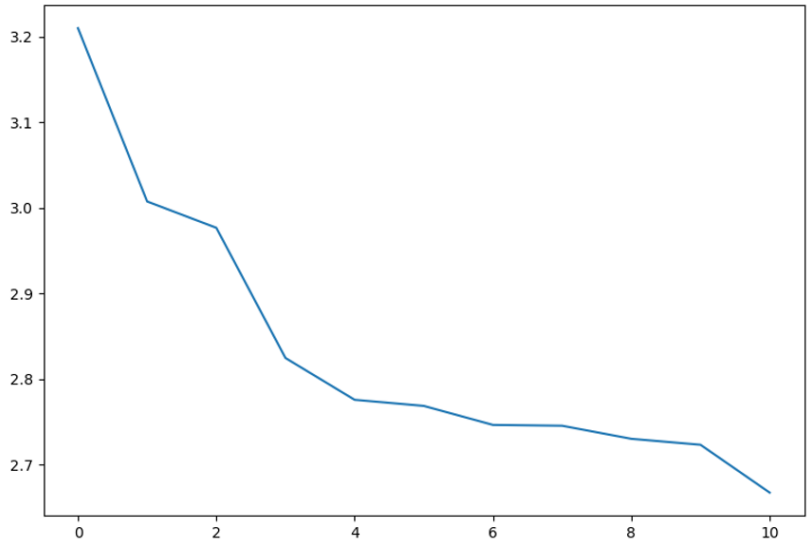

(g) Patient 9. Final BP score = 2.668, $\triangle$BP = 0.543

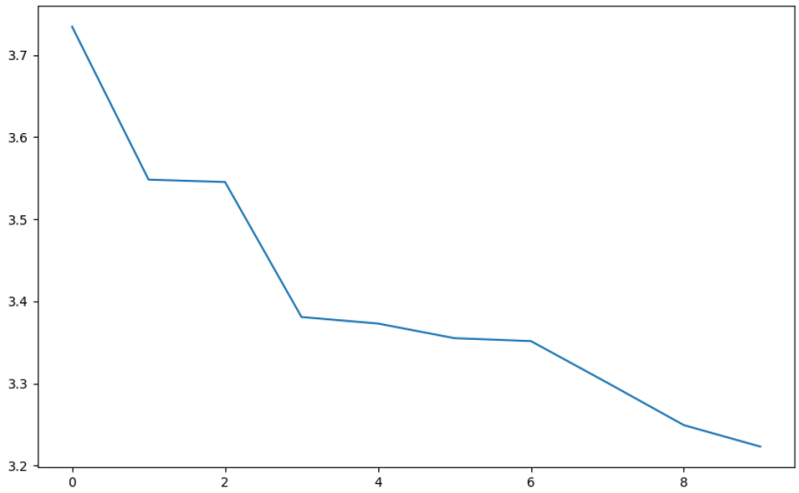

(h) Patient 10. Final BP score = 3.223, $\triangle$BP = 0.507

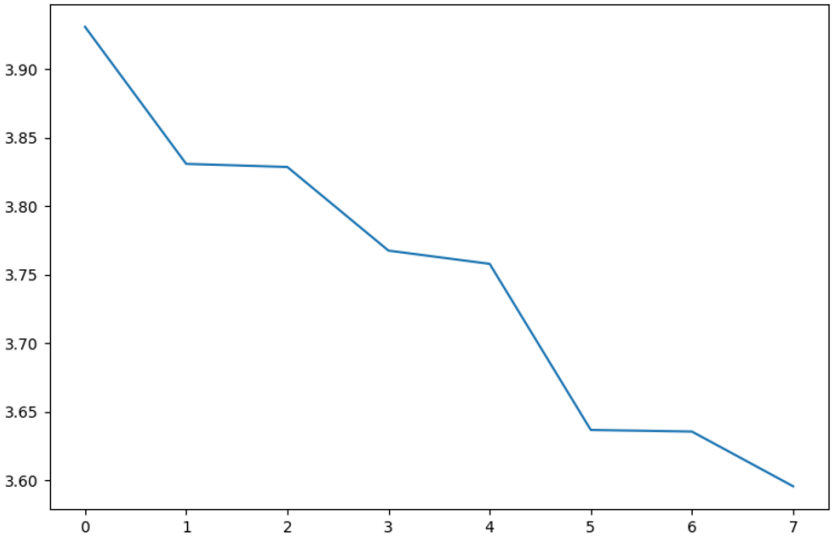

(i) Patient 11. Final BP score = 3.600, $\triangle$BP = 0.333

Figure B.1: Decrease in Bone Protrusion score throughout optimization.
y-axis = BP score, x-axis = incidence of decrease in BP

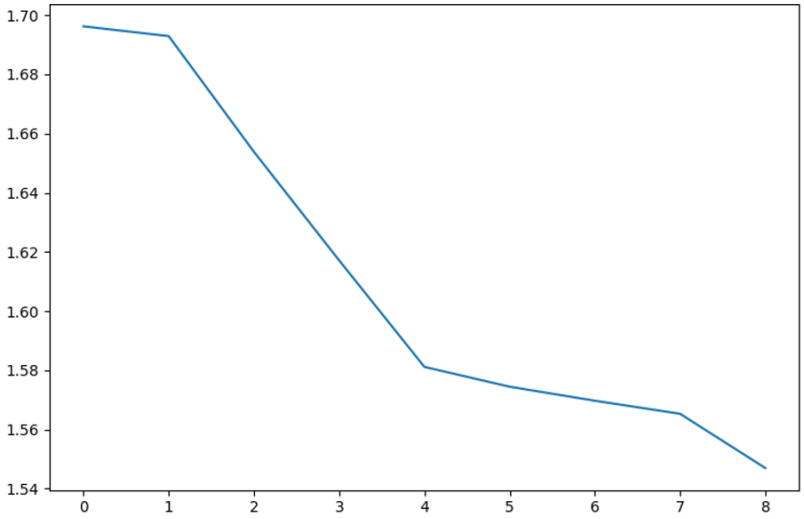

(j) Patient 12. Final BP score = 1.547, $\triangle$BP = 0.149

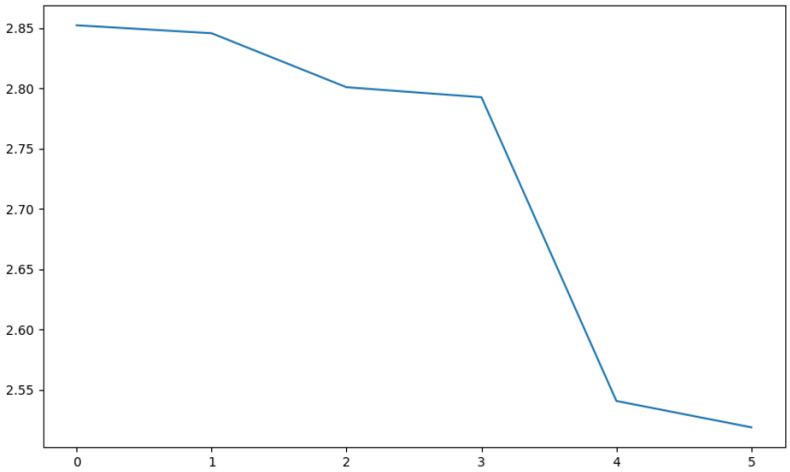

(k) Patient 14. Final BP score = 2.519, $\triangle$BP = 0.333

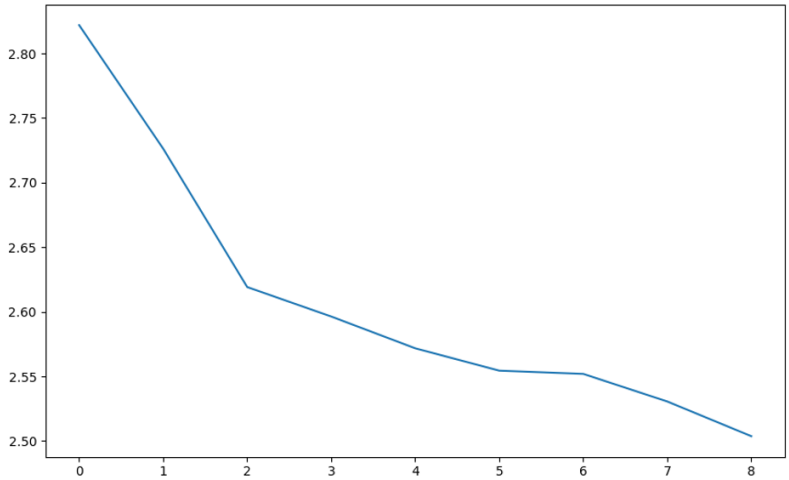

(l) Patient 15. Final BP score = 2.504, $\triangle$BP = 0.317

Figure B.1: Decrease in Bone Protrusion score throughout optimization.
y-axis = BP score, x-axis = incidence of decrease in BP